Single-molecule detection of transient dimerization of opioid receptors 2: Heterodimer blockage reduces morphine tolerance

Peng Zhou[1], Rinshi S. Kasai[2,3,4], Wakako Fujita[5,6], Taka A. Tsunoyama[1], Hiroshi Ueda[7,8], Simone Pigolotti[9], Takahiro K. Fujiwara[10], and Akihiro Kusumi[1,10]

[1]Membrane Cooperativity Unit, Okinawa Institute of Science and Technology Graduate University, Onna-son, Okinawa 904-0495, Japan. [2]Institute for Life and Medical Sciences, Kyoto University, Kyoto 606-8507, Japan. [3]Division of Advanced Bioimaging, National Cancer Center Research Institute, Tokyo 104-0045, Japan. [4]Institute for Glyco-core Research (iGCORE), Gifu University, Gifu 501-1193, Japan. [5]Department of Medical Pharmacology, Nagasaki University Graduate School of Biomedical Sciences, Nagasaki 852-8520, Japan. [6]Laboratory of Pharmacotherapeutics, Faculty of Pharmacy, Juntendo University. Urayasu, 279-0013, Japan. [7]Laboratory for the Study of Pain, Research Institute for Production Development, Kyoto 606-0805, Japan. [8]Department of Pharmacology, National Defense Medical Center, Nei-Hu 114, Taipei, Taiwan. [9]Biological Complexity Unit, Okinawa Institute of Science and Technology Graduate University, Onna-son, Okinawa 904-0495, Japan. [10]Institute for Integrated Cell-Material Sciences (WPI-iCeMS), Kyoto University, Kyoto 606-8501, Japan.

Abstract

Heterodimerization of opioid receptors (ORs), MOR, KOR, and DOR, is implied in their functional regulation and diversification, and thus its understanding is crucial for developing better analgesic treatments. However, our knowledge on OR heterodimerization/heterodimers remains limited. Here, using single-molecule imaging and functional analysis, we found that MOR, the main morphine receptor, repeatedly forms *transient (≈250 ms) heterodimers* with DOR every 1-10 seconds, but not with KOR, whereas DOR and KOR also form transient heterodimers. We obtained all the heterodimer-monomer equilibrium constants and rate constants with/without agonists. We identified the critical heterodimer binding sites in the extracellular domains, in addition to the less-specific transmembrane domains, and developed soluble peptide blockers for MOR-DOR and DOR-KOR heterodimerization, using amino-acid sequences mimicking the extracellular binding sites. With these peptide blockers, we dissected the monomer/dimer roles in OR internalization and signaling. The soluble MOR-DOR heterodimer blocker reduced the development of long-term morphine tolerance in mice.

Introduction

As elucidated in our companion paper,[1] the transient homodimerization of μ-, κ-, and δ-opioid receptors (KOR, MOR, and DOR, respectively) provides a critical layer of regulation within the opioid signaling paradigm. New theories and methods for quantitative analyses of single-molecule imaging data developed there revealed that all ORs undergo transient homodimerizations for brief periods of 120-180 ms (k_{off} = 6.7-8.5 s^{-1}), and they repeat dissociation and rebinding to another molecule every few seconds or less under physiological expression levels, with homodimer-dissociation equilibrium constants of 5.9-16.4 copies/μm^2. The homodimerization is predominantly driven by unique 9-26 amino-acid stretches within the C-terminal cytoplasmic domain of each receptor, with less specific contributions from the transmembrane (TM) domains. Soluble but membrane-permeable peptides mimicking these C-terminal regions reduced homodimerization, enabling us to dissect the functions of homodimers. Compared to their monomeric counterparts, KOR-KOR and DOR-DOR homodimers (KK and DD homodimers)—unlike MOR-MOR homodimers (MM homodimers)—activate downstream signals differently in response to agonist binding, without affecting receptor internalization.

In this paper, we extend these advanced single-molecule imaging studies described in the companion paper to investigate OR *hetero*dimerization. The heterodimerization of three classical ORs introduces a new dimension to receptor interactions with G proteins, GRKs, and arrestins,[2, 3, 4, 5, 6] providing additional opportunities for modulating OR functions. This modulation could be clinically utilized for managing chronic pain and treating neuropsychiatric disorders.[7, 8, 9, 10]

Given its crucial role in morphine response and the significant medical and social implications thereof, MOR has been the focus of extensive OR research,[10, 11, 12, 13, 14, 15] including its heterodimerization with DOR and KOR (DM and KM heterodimers, respectively).[10, 13, 16, 17] Extensive studies have reported DM heterodimerization[3, 18, 19, 20] and downstream signals suggesting DM interactions,[21, 22, 23, 24] although DM co-expression might be limited to small populations of neurons, such as excitatory interneurons, projection neurons in the spinal cord

66 dorsal horn, and nociceptive neurons in dorsal root ganglia.[23, 25, 26] In contrast, evidence for KM
67 heterodimerization remains sparse, which suggests a dependence on the physiological
68 context.[17, 27, 28]

69 The DK coupling exhibited unique signaling and functional regulation, making the DK
70 heterodimer as another promising therapeutic target for pain treatment.[11, 29, 30] Indeed, DK
71 heterodimerization and observations suggesting DK interactions have also been reported,[11, 28,
72 29, 31, 32] further highlighting its significance.

73 Despite these studies, the fundamental properties of heterodimers, including
74 heterodimer-monomer dissociation equilibrium constants and rate constants (K_D, k_{off}, which is
75 inverse lifetime, and k_{on}), heterodimer interaction sites, and cellular- and tissue-level functions,
76 remain enigmatic. This research addresses these fundamental issues by leveraging the
77 advanced single-molecule image analysis described in the companion paper. Such
78 understanding would form the basis for developing opioid analgesics with heightened efficacy
79 and minimized tolerance.

80 The heterodimer-monomer equilibrium constant, K_D (hetero-K_D), can only be obtained
81 after the homodimer-monomer equilibrium constants K_Ds (homo-K_Ds) for the two constituent
82 ORs are evaluated, as detailed in the companion paper. We also compare the properties and
83 dimerization sites between homo- and hetero-dimers of ORs.

84 This study lays the groundwork for future explorations of dimerization phenomena across
85 the broader GPCR family.[33, 34] Heterodimerization among class-A GPCRs has been increasingly
86 observed, offering insights into novel signaling pathways and pharmacological profiles.[7, 8, 16, 35,
87 36] Examples include heterodimers between MOR and V1b vasopressin receptor,[37] MOR and
88 somatostatin receptor 2,[38] dopamine D2 receptor and neurotensin NTS1 receptor,[39] angiotensin
89 II AT1 receptor and norepinephrine α2C-adrenergic receptor,[35] cannabinoid receptors CB1 and
90 CB2,[40] dopamine receptors D1 and D2,[41] and others, marking an emergent frontier in GPCR
91 research with profound implications for drug discovery.

Here, we unequivocally demonstrate that, under low physiological expression conditions, DOR-MOR and DOR-KOR form metastable heterodimers, whereas MOR-KOR heterodimers are not detectable. These findings have been substantiated through examinations conducted with a level of quantification unparalleled in the existing biomedical literature, with the exception of the OR homodimer research described in our companion paper.

Furthermore, we discovered that the extracellular N-terminal domain interactions and extracellular loop 3 (EL3) interactions are specifically responsible for DM and DK heterodimerizations, respectively. In contrast, the TM domain interactions contribute less specifically, challenging the common belief that GPCR dimerizations are primarily mediated by TM domain interactions.[3, 16, 30, 42, 43, 44] In addition, allosteric conformational changes involving both extracellular domains and TM domains might be involved.

Building on these findings, we demonstrated that soluble peptides mimicking the extracellular amino-acid sequences implicated in DM and DK heterodimerizations effectively inhibit heterodimer formation. In murine models, the administration of a soluble peptide blocker targeting the DM heterodimers into the cerebral ventricles diminishes the development of long-term morphine tolerance. These results strongly suggest that DM heterodimerization based on the N-terminal domain sequence occurs in neuronal tissues. These findings underscore potential avenues for improving opioid drug administration strategies aimed at mitigating tolerance and dependence.

112 # Results

113 **Metastable DM and DK, but not MK, heterodimers are detected in the PM**

114 SNAPf-ORs and OR-Halos were expressed in CHO-K1 cells, which do not express ORs
115 (Supplementary Fig. 1a).[45] These tagged ORs are functional (Supplementary Fig. 1a, b) and
116 labeled with SNAP-Surface 549 and Halo7-SaraFluor650T dyes. Their fluorescence
117 characteristics are summarized in Supplementary Fig. 1c-e. The labeled OR molecules were
118 simultaneously observed in two colors at the single molecule level at video rate (30 Hz) at 37°C,
119 using a home-built total internal reflection fluorescence (TIRF) microscope. The cells expressing
120 each OR species at fluorescence spot densities between 0.5-1 spot/μm^2 (total number densities
121 between 1-2 spots/μm^2) after fluorescence labeling were selected for microscope observations.
122 Virtually all of the OR fluorescent spots exhibited diffusion in the PM.

123 When DOR and MOR were expressed in the same cell, they exhibited frequent brief
124 colocalization and co-diffusion, suggesting metastable DM heterodimer formation
125 (Supplementary Videos 1 and 2; Fig. 1a). For quantifying colocalization, we employed a pair
126 cross-correlation function (PCCF; Supplementary Fig. 1f; also see companion paper), which
127 provides both a simple measure for heterodimer formation, the colocalization index, and a
128 fundamental constant, the heterodimer-monomer dissociation equilibrium constant K_D (see
129 Supplementary Note 2, Supplementary Fig. 2e, and related main text of the companion paper).
130 As a control for incidental fluorescent spot colocalizations, the video frames in the green
131 channel were rotated 180° before overlaying (see Supplementary Fig. 2d of the companion
132 paper).

133 The colocalization index clearly indicated that DOR and MOR form DM heterodimers (Fig.
134 1b) and DOR and KOR form DK heterodimers (Fig. 1b and Supplementary Fig. 1f) in the PM
135 (all statistical parameters including *p* values and numbers of replicates are summarized in
136 Supplementary Table 1). However, at the expression levels employed in this study, KM
137 heterodimers were not detected (Fig. 1b and Supplementary Fig. 1f), consistent with the

138 previous result.[28] The heterodimer-monomer dissociation equilibrium constants K_D's were
139 obtained from the PCCFs (Fig. 1c).

140 The heterodimer lifetime (τ_2) was determined from k_{off} (summarized in Fig. 1c), evaluated
141 from the distribution of colocalization *durations* (Fig. 1d; see Note S1 in the companion paper).
142 The τ_2 values are 260 ± 12 ms for DM heterodimers and 241 ± 10 ms for DK heterodimers,
143 after corrections for trackable duration lifetimes (Fig. 1d and Supplementary Fig. 1e). The
144 histogram for the MK colocalization durations did not exhibit any τ_2 component (the decay
145 component representing the heterodimer loss), consistent with the lack of detectable
146 heterodimers for this pair (only incidental colocalization with a lifetime of τ_1; Fig. 1d).

147 To identify the amino-acid sequences responsible for specific heterodimerization, we
148 initially examined the OR domains with lower amino-acid identities/homologies among the three
149 ORs. The candidate sites we initially selected are summarized in Fig. 1e. The amino-acid
150 sequence homologies in the cytoplasmic C-terminal domains are lower, but they are not
151 included in this figure as they are involved in KK, MM, and DD homodimerizations (companion
152 paper) and we unequivocally showed that they are not involved in DK and DM
153 heterodimerizations (Fig. 2a and 3a).

154

155 **DOR's EL3, TM1, and TM4, but not EL2, N- or C-terminal domain, contribute to DK**
156 **heterodimerization**

157 We first examined heterodimerization of wild-type (WT) KOR and N- or C-terminal deletion
158 mutants (ΔN or ΔC mutants) of DOR (Fig. 2a, Top). We found that DOR's N- and C-terminal
159 domains are not involved in DK heterodimerization, and KOR's ΔN or ΔC mutations are not
160 involved in heterodimerization with WT-DOR (Fig. 2a, Bottom). These results indicate that DK
161 heterodimerization involves neither the N- nor C-terminal domains of DOR and KOR.

162 Given the scarce occurrence of MK heterodimers (colocalization index = 1.15 ± 0.03), we
163 tested whether MOR mutants with some domains substituted with DOR counterparts could
164 heterodimerize with WT-KOR (Fig. 1e; see Fig. 2b for domain names and amino-acid numbers;

165 results shown in Fig. 2c left). Substitution with DOR's TM1 or TM4 domain in MOR (MOR[TM1^{DOR}]
166 or MOR[TM4^{DOR}]) facilitated heterodimer formation with WT-KOR, qualitatively consistent with
167 a previous result.[30] However, replacing MOR's EL2 or N-terminal domain (MOR[EL2^{DOR}] or
168 MOR[Nterm^{DOR}]) did not induce heterodimerization with WT-KOR. Meanwhile, introducing
169 DOR's EL3 domain into MOR (MOR[EL3^{DOR}]) resulted in heterodimerization with WT-KOR. These
170 results indicate the involvement of DOR's EL3 domain, alongside its TM1 and TM4 domains, in
171 DK heterodimer formation.

172 The lifetime distribution for the MOR(EL3^{DOR})-KOR heterodimer revealed the appearance
173 of the τ_2 component, which did not exist in that for the MK pairs (Supplementary Fig. 2).
174 Although the τ_2 value is smaller than that for WT-DK heterodimers (164 ± 25 ms vs. 241 ± 9.7
175 ms), this result further suggests that DOR's EL3 domain is involved in DK heterodimerization.

176 Experiments replacing various DOR domains with the MOR counterparts and examining
177 heterodimerization with WT-KOR (based on the lack of MK heterodimerization) showed reduced
178 heterodimerization for TM1, TM4, and EL3 domain replacements, but not for EL2 or N-terminal
179 domain substitutions (Fig. 2c right). This further indicates that DOR's EL3, TM1, and TM4
180 domains are integral to DK heterodimer formation.

181

182 **Soluble EL3-domain peptides of DOR and KOR both block DK dimerization**

183 A variety of deletions (Fig. 2a) and substitutions (Fig. 2c) introduced into WT-DOR could alter
184 its conformation, which might affect true interaction sites, leading to the reduction of DK
185 heterodimerization. To study this aspect, we synthesized soluble peptides with the EL3
186 sequences of DOR and KOR (Fig. 1e). Addition of either peptide (1 μM, final concentration) to
187 cells co-expressing DOR and KOR significantly reduced DK heterodimerization, unlike the
188 peptide with the MOR EL3 sequence (Fig. 2d). This highlights the critical roles of the DOR and
189 KOR EL3 domains in DK heterodimerization. Given that DOR's EL2 domain and the N-terminal
190 domains of both DOR and KOR are not involved in DK heterodimerization (Fig. 2a, c), these

191 results indicate that the interaction between the DOR and KOR EL3 domains is crucial for DK
192 heterodimerization, although that with KOR's EL2 domain has not been ruled out.
193 Furthermore, we found that DOR's TM1 and TM4 peptides expressed in the PM became
194 colocalized with KOR, supporting their involvement in DK heterodimerization (Fig. 2b, e). These
195 results are consistent with those shown in Fig. 2c and a previous observation,[31] and indicate
196 that the interactions between the DOR and KOR EL3s, and those of DOR's TM1 and TM4 with
197 KOR's TM domains are involved in DK heterodimerization.
198
199 **DM dimerization is predominantly mediated by N-terminal domain interactions**
200 To identify the amino-acid sequences responsible for DM heterodimerization, first, we
201 systematically deleted partial sequences from the N- and C-terminal domains of DOR and MOR
202 (Fig. 3a). We found that DOR's N-terminal amino acids 22-42 (with the critical amino acids 22-
203 27) and MOR's N-terminal amino acids 32-61 play key roles in DM heterodimerization, likely by
204 binding to each other (Fig. 3a). The key DOR sequence was further confirmed by replacing
205 DOR's amino acids 21-27 with an arbitrarily selected amino-acid sequence, rather than deleting
206 the original sequence (Supplementary Fig. 3). Therefore, these sequences are likely to be the
207 binding interfaces for DM heterodimerization. However, the colocalization index did not
208 decrease to 1 (but to 1.15, as found for MK heterodimerization), probably due to the presence
209 of other binding sites such as TM domains, as suggested previously (see below).[3, 43, 46]
210 The histograms of the colocalization *durations* for DORΔ22-42 with WT-MOR and
211 MORΔ32-61 with WT-DOR both revealed only small fractions of the τ_2 components, with
212 significantly reduced heterodimer lifetimes of 88 ± 12 ms and 91 ± 8 ms, respectively (Fig. 3b).
213 These shorter lifetimes (≈90 ms), compared to the 260-ms lifetime of the WT DM heterodimers,
214 might represent the lifetimes of DM heterodimers induced by the less-stable TM domain
215 interactions.
216 We further explored the specific regions mediating DM heterodimerization by taking
217 advantage of the fact that MK heterodimerization hardly occurs at the expression levels we

218 employed. Thus, we examined WT-MOR interactions with DOR mutants with various DOR
219 domains substituted with their KOR counterparts (Fig. 3c left). The colocalization index upon
220 replacement of the N-terminal domain substantially decreased, consistent with the previous
221 demonstration that the N-terminal domains of DOR and MOR are instrumental in DM
222 heterodimer formation (Fig. 3a, b).

223 Substitution of DOR's TM1 or TM4 with its KOR counterpart, but not TM6 (Fig. 1e), yielded
224 moderate reductions in colocalization with WT-MOR, but not as much as the N-terminal domain
225 substitution (with $Nterm^{KOR}$), suggesting that DOR's TM1 and TM4 play ancillary roles in DM
226 heterodimer stability (Fig. 3c left). These results, but not that of TM6, are consistent with
227 previous computational modeling predictions.[43, 46] The DOR mutant bearing the three
228 replacements of KOR's N-terminal domain, TM1, and TM4 exhibited a lower colocalization index
229 with WT-MOR, comparable to that for the MK hetero-pair (1.15).

230 Conversely, the replacement of MOR's N-terminal domain with that from KOR (with
231 $Nterm^{KOR}$) greatly reduced the colocalization with DOR (Fig. 3c right). This result further
232 supports the idea that the major interaction sites for DK dimerization do not involve the N-
233 terminal domains, but the key interactions occur between the EL3 domains as well as TM
234 domains in DOR and KOR (Fig. 2). Importantly, it further demonstrates that the predominant
235 interactions for DM heterodimerization occur between the N-terminal domains of both DOR and
236 MOR (Fig. 3a, b). The interactions of the N-terminal domains with the EL2 and EL3 domains
237 would be far less important for DM heterodimerization than those between the DOR and MOR
238 N-terminal domains, because the lack of either DOR residues 22-42 or MOR residues 32-61 is
239 sufficient to significantly lower the colocalization index (Fig. 3a) and eliminate the second
240 colocalization lifetime component (Fig. 3b).

241

242 **TM interactions enhance both homo- and hetero-dimerizations of ORs**

243 The results described in the previous subsection further support the involvement of DOR's TM1
244 and TM4 in both DM (Fig. 3c left) and DK (Fig. 2c, left and right, and e) heterodimerizations.

245 Furthermore, MOR's TM1 participates in both DM heterodimerization and MM homodimerization
246 (Fig. 5b-e in companion paper; Fig. 5 of this paper). These results suggest that the TM
247 interactions support both homo- and hetero-dimerizations of ORs; namely, the TM interactions
248 are less specific. This finding is aligned with previous controversial reports: The conclusion we
249 obtain from the reported results in the literature is that the same TM domains contribute to
250 both homo- and hetero-dimerizations of ORs and other GPCRs to various extents.[43, 44, 46, 47, 48]
251

252 **Soluble N-terminal-domain peptides block DM heterodimerization**

253 We then utilized the soluble peptides corresponding to the N-terminal sequences of both DOR
254 and MOR implicated in DM heterodimerization, as we did for confirming the DK heterodimer
255 binding sites (EL3 domains of both molecules; Fig. 2d). These soluble peptides from DOR and
256 MOR are called Dpep(m-n)DM and Mpep(m-n)MD, respectively, where m and n indicate the
257 amino acid numbers in the original OR sequences (see "Location in DOR" and "Location in MOR"
258 in Fig. 4a, respectively). Among the various DpepDMs and MpepMDs, Dpep(20-42)DM and
259 Mpep(32-61)MD most potently lowered the colocalization indexes to 1.2-1.3 (Fig. 4a), mirroring
260 the effects observed with the deletion and replacement mutants (Fig. 3a, c).

261 The colocalization index for DM heterodimers decreased with an increase in the Dpep(20-
262 42)DM concentration (Fig. 4b), indicating that the affinity of the DM heterodimers is $K_D \approx 0.1$
263 μM in three-dimensional space. This 3D concentration could not readily be converted to a two-
264 dimensional molecular density, as discussed in the companion paper (main text explaining Fig.
265 5a-d). Briefly, in two-dimensional space, the dimerization efficiency is far greater, by a factor
266 of 10^6, than that in three-dimensional space.[49] Therefore, the efficacy of the peptides in
267 blocking OR dimerization, even at the 0.1 μM-order concentrations required for blocking DM
268 heterodimerization, is deemed plausible given the nanomolar affinity range of OR ligands (1-
269 10 nM).

270 Dpep(20-42)DM's introduction substantially shortened the DM heterodimer lifetime from
271 260 ms to 124 ms (Fig. 4c), supporting that the amino acid sequence 20-42 in DOR is critical

272 for DM heterodimer formation. The shortened lifetime might reflect heterodimer facilitation by
273 the TM domains.
274

275 **The membrane-integral peptide TM1^{MOR} suppresses both DM heterodimerization**
276 **and MM homodimerization**

277 Next, we examined whether MOR's TM1 (TM1^{MOR}) is involved in DM heterodimerization, as
278 previously described.[3, 43, 46] In addition to TM1^{MOR} (amino acids 71-99), a second construct
279 containing amino acids 53-70 before the TM1 domain (Nterm- TM1^{MOR}) was used (see Fig. 2b
280 for construct names and exact amino-acid ranges), following a previous report.[3] When these
281 peptides were co-expressed with DOR, both TM1^{MOR} and Nterm-TM1^{MOR} colocalized with DOR,
282 like the full-length MOR (all molecules expressed at densities of 0.5-1.0 fluorescent spots/μm^2;
283 Fig. 5a, b). These TM1 constructs also suppressed DM heterodimerization in an expression
284 level-dependent manner, indicating TM1^{MOR}'s significant contribution to the DM interaction (Fig.
285 5c).

286 Notably, the addition of either Dpep(20-42)DM (also Mpep(32-61)MD) or TM1^{MOR} alone
287 reduced the colocalization index to near-baseline levels (1.2-1.3) (Fig. 4a, b and 5c). These
288 results suggest that DM heterodimerization might not be induced by simple bindings at two
289 sites, but instead mediated by cooperative allosteric conformational changes of the extracellular
290 N-terminal domains and TM domains in both OR molecules. In this case, our description of the
291 dynamic dimer-monomer equilibrium should be considered as a simplified representation of the
292 actual molecular events.

293 To identify the DOR's TMs interacting with MOR, we examined the colocalization of WT-
294 MOR with TM1^{DOR} and TM4^{DOR}, which were previously suggested to interact with TM1^{MOR}.[43, 46]
295 TM1^{DOR} and TM4^{DOR} moderately colocalized with MOR when expressed at similar levels (both
296 at densities of 0.5-1.0 fluorescent spots/μm^2; Fig. 5b). Furthermore, TM4^{DOR} suppressed DM
297 heterodimerization in an expression level-dependent manner, but not as much as TM1^{MOR} (Fig.
298 5c), indicating its contribution to DM heterodimerization but also suggesting the presence of

299 other significant binding sites, including $TM1^{DOR}$ and other TM domains as well as the N-terminal
300 domain.

301 Despite these findings, we emphasize the critical role played by the interactions of the N-
302 terminal domains of DOR and MOR. This is because the TM interactions are not quite specific,
303 as described. Namely, $TM1^{DOR}$ and $TM4^{DOR}$ are involved in both DM (Fig. 3c left) and DK (Fig.
304 2c, left and right, and e) heterodimerizations, and $TM1^{MOR}$ is involved in both DM
305 heterodimerization (Fig. 3c right; Fig. 5d as it blocks DD homodimerization) and MM
306 homodimerization (Fig. 5d; also refer to Fig. 5b-e in companion paper). In striking contrast,
307 Dpep(20-42)DM had no influence on either MM or DD homodimerization (Fig. 5d). A control
308 TM-peptide, TM^{LDLR}, with the sequence of the LDL receptor's TM domain, exhibited no effect
309 on homodimer blocking (Fig. 5d).

310 In conclusion, the N-terminal domains of DOR and MOR are specifically involved in DM
311 heterodimerization, whereas the TM domains contribute but interact less specifically: $TM1^{MOR}$
312 in MOR enhances both DM heterodimerization and MM homodimerization, and $TM1^{DOR}$ and
313 $TM4^{DOR}$ in DOR participate in both DM and DK heterodimerization. Meanwhile, DM
314 heterodimerization might involve allosteric interactions between the N-terminal and TM
315 domains.

316

317 **M-agonists' effect on DM heterodimerization**

318 We examined the effects of MOR agonists (M-agonists), morphine and [D-Ala2, N-MePhe4, Gly-
319 ol]-enkephalin (DAMGO), on DM heterodimerization (Fig. 6a-e). At an M-agonist concentration
320 of 0.5 μM in the cell culture medium, MOR would be rapidly bound by morphine and DAMGO
321 (denoted as M^{*mor} and M^{*DAMGO}, respectively),[50] and therefore we examined the M-agonist
322 effect on DM heterodimerization within 5 min after the agonist addition, prior to any detectable
323 internalization. As detailed in the companion paper, DAMGO enhanced MM *homo*dimerization
324 and slightly elongated the MM dimer lifetime (Fig. 5c and d, respectively, in companion paper).

325 M*^{mor} exhibited almost the same colocalization index with DOR as non-ligated MOR,
326 although the DM*^{mor} heterodimer lifetime was shorter (Fig. 6a-c). The effects of Dpep(20-42)
327 on DM dimerization for M*^{mor} and non-ligated MOR were very similar (Fig. 6a, b, and e).
328 M*^{DAMGO} exhibited a greater colocalization index with DOR (DM*^{DAMGO} heterodimers) with a
329 prolonged heterodimer lifetime, compared to MOR in the basal state (Fig. 6a-e). The presence
330 of Dpep(20-42)DM in the medium markedly reduced both the colocalization index and lifetime
331 of the DM*^{DAMGO} heterodimers. The influence of the DOR agonist, 0.5 μM SNC-80, on MOR and
332 SNC-80-bound DOR heterodimerization could not be determined due to the rapid internalization
333 of MOR and DOR after SNC-80 addition, as reported in subsequent sections.
334

335 **Summary of K_D, k_{off}, and k_{on} values and expected percentages of OR protomers**
336 **existing as homo- and hetero-dimers at various expression levels**

337 The equilibrium constants K_Ds were deduced by fitting the experimental PCCF histograms for
338 DM and DK heterodimers with theoretical models (Fig. 6a), using hetero-K_D and σ as fitting
339 parameters (Eqs. 26 and 73-75 in Supplementary Note 2 in companion paper for homodimer).
340 The derived K_D, k_{off}, and k_{on} values for KK, MM, and DD homodimers as well as DM and DK
341 heterodimers, with or without M-agonists and Dpep(20-42)DM, are summarized in Fig. 6d and
342 e (for the influence of expression levels on the evaluated K_D values with actual curve fitting
343 results, see Supplementary Fig. 4a-d; for the SEM, see Supplementary Tables 2 and 3; all
344 statistical data are summarized in Supplementary Table 1).

345 Based on the K_D values obtained here, the percentages of OR protomers existing as
346 monomers, DD and MM homodimers, and DM and DK heterodimers in the presence and
347 absence of morphine and DAMGO, at various number densities of ORs expressed in the PM,
348 are calculated and shown in Fig. 7 and Supplementary Tables 2-4 for the cases where DOR and
349 MOR expression levels are equalized. In particular, Supplementary Table 4 presents the
350 fractions of MOR or DOR protomers existing as monomers, homodimers, and heterodimers. For

351 the cases where expression levels are freely varied, see Fig. 7. Without knowing the K_D values
352 for both homo- and hetero-dimerizations, such evaluations would have been impossible.
353

354 **Virtually all OR molecules alternate between existing as homo- and hetero-dimers**
355 **and monomers during short periods on orders of 1-10 s**

356 Cautious interpretations are required for the small percentages of OR protomers, 4.2-21.2%,
357 existing as homo- and hetero-dimers at any moment at low physiological expression conditions
358 (1 copy/μm^2 for each OR; see columns of expression levels of 1 copy/μm^2 and 1+1 copies/μm^2
359 in Supplementary Tables 2 and 3, respectively; including the presence of morphine and DAMGO,
360 but not peptide dimer blockers). Based on these values, one might consider the functional
361 influence of dimers to be small, but this would be incorrect. Note that the dimer lifetimes are
362 in the range of 118-369 ms, indicating that these dimers fall apart quickly, but then the
363 monomers will again form dimers with different (and sometimes the same) partner molecules
364 (see Supplementary Fig. 2a and b in companion paper for an example). This process is
365 continually repeated. Therefore, although at any time the percentages of protomers existing
366 as dimers are limited, virtually all OR molecules rapidly interconvert among homodimer-,
367 monomer-, and heterodimer-states and monomers during short periods on orders of 1-10 s (at
368 physiological expression levels for both molecules) (Fig. 6e and Supplementary Table 3).

369 This indicates that ORs would perform their functions while undergoing rapid monomer-
370 dimer interconversions. If the functionalities of monomers and dimers are different, this raises
371 the possibility to fine-tune the OR functions by modulating monomer-dimer interconversions by
372 natural agonists and synthetic drugs.
373

374 **Lack of morphine-induced internalization of MOR and DOR even in MD cells**

375 Transient DM heterodimerization might affect agonist-induced intracellular signaling and
376 internalizations of MOR and DOR, and thus analgesic efficacy and tolerance development (Fig.
377 8a). Therefore, we examined the effects of DM heterodimerization on downstream signals after

378 M-agonist stimulation and the internalization of MOR and DOR before and after M- and D-
379 agonist stimulation (0.5 μM), using three cell lines produced here: (1) M-cells, CHO-K1 cells
380 stably expressing SNAPf-MOR at 0.5-1.0 fluorescent spots/μm^2 after labeling with SNAP-
381 Surface 549; (2) D-cells, CHO-K1 cells stably expressing SNAPf-DOR at 0.5-1.0 fluorescent
382 spots/μm^2 after labeling with SNAP-Surface 549; (3) MD-cells based on M-cells (or D-cells),
383 transiently transfected with the cDNA encoding DOR-Halo (or MOR-Halo), which was labeled
384 with SaraFluor 650T (cells exhibiting 0.5-1.0 fluorescent spots/μm^2 were selected for
385 observations). The two types of MD-cells (based on M-cells or D-cells) are biologically the same
386 (thus, in the following, we simply call them MD-cells), apart from the experimental details (i.e.,
387 for the assay of MOR and DOR internalizations, SNAPf-MOR and SNAPf-DOR must be used,
388 respectively, because our assay depends on the quenching of fluorescence signal from these
389 molecules located on the cell surface using the membrane impermeable quencher; see below
390 and the companion paper). Dpep(20-42)DM (1 μM) was extensively used to dissect the
391 functions of DM heterodimers from those of D/M monomers and DD/MM homodimers.

392 The time courses of OR internalizations were monitored for 55 min by measuring the OR
393 molecules remaining in the PM. The OR amounts in the PM were measured by TIRF microscopy,
394 by evaluating the signal intensities of the OR molecules in the TIRF illumination range (in PM
395 plus cytoplasm within ≈100 nm from the PM) before and after the addition of a membrane-
396 impermeable fluorescence quencher, Mn(III) meso-tetra(4-sulfonatophenyl)porphine (Mn^{3+}-
397 TSP) (i.e., the intensity of the fluorescence signal from the cytoplasm in the TIRF illumination
398 range), and then subtracting the latter from the former (see Fig. 6a and Supplementary Fig. 6
399 and related main text in the companion paper; also see Methods). Each time course obtained
400 under various conditions could be fitted with a single exponential function plus a constant. The
401 constant provided the OR fraction whose internalization is undetectable within 55 min, and the
402 exponential decay constant provided the residency lifetime in the PM for the OR's internalized
403 fraction observed during 55 min (Fig. 8b and Supplementary Fig. 5; for summaries and
404 statistical test results see Supplementary Table 5).

405 MOR internalization before and after morphine addition was hardly detectable in either
406 M- or MD-cells (Fig. 8b, Left column, Top and middle; Supplementary Fig. 5, Top and third
407 rows). These results indicate that the internalization of DM heterodimers is as slow as that of
408 MOR monomers and homodimers and their internalization rates are not affected by morphine
409 binding. This was further confirmed by the lack of Dpep(20-42)DM effects on M and M^{*mor}
410 internalization (Fig. 8b, Left column, Top and middle; Supplementary Fig. 5, Top-fourth rows).
411 DOR internalization was similarly unaffected by morphine addition in MD-cells (Fig. 8b, Right
412 column, Top and middle; Supplementary Fig. 5, Top-fourth rows).
413 However, these observations require cautious interpretations due to the low fractions of
414 M and M^{*mor} existing as DM and DM^{*mor} heterodimers, respectively, under the employed
415 expression levels (≈5% as shown in Supplementary Table 3; see the column of 1+1 copies/μm^2;
416 i.e., the case approximating experimental observation conditions of 0.5-1.0 fluorescent
417 spots/μm^2 for both SNAPf-MOR and DOR-Halo), although, as described in the previous
418 subsection, virtually all OR molecules would experience dimer periods within 1-10 s. In certain
419 PM domains in some neurons, the MOR and/or DOR concentrations may far exceed those used
420 in this study (e.g., MOR in primary cilia),[51] and the morphine effect on the MM and/or DM dimer
421 internalizations could be more pronounced.
422

423 **Highly-enhanced M^{*DAMGO} internalization during transient binding to DOR**

424 In contrast to morphine, DAMGO administration resulted in pronounced internalization of
425 DAMGO-bound MOR (M^{*DAMGO}) in both M- and MD-cells (Fig. 8b, Left column, Bottom;
426 Supplementary Fig. 5, Fifth and sixth rows; Supplementary Table 5). The results in M-cells are
427 virtually the same as those reported in the companion paper (Fig. 6b, Middle column and Table
428 1), which show significant M^{*DAMGO} internalization during 35 min (55 min for the results shown
429 here) that is not influenced by $M^{*DAMGO}M^{*DAMGO}$ homodimerization.
430 In MD-cells, the proportion of internalized M^{*DAMGO} is higher compared to that in M-cells
431 (48% vs. 30%). This difference occurs despite the low fractions of M^{*DAMGO} existing as

432 DM*^{DAMGO} heterodimers (9.1% at time 0) (Supplementary Table 3; see the 1+1 copies/μm^2
433 column). The addition of Dpep(20-42)DM to MD-cells, which reduces heterodimeric M*^{DAMGO}
434 from 9.1% to 4.3% (Supplementary Table 3), significantly reduced M*^{DAMGO} internalization from
435 48% to 26% (Fig. 8b and Supplementary Table 5). Therefore, we conclude that significant
436 M*^{DAMGO} internalization occurs with DM*^{DAMGO} heterodimers in addition to M*^{DAMGO} monomers
437 and homodimers. Although the co-internalization of MOR and DOR following DAMGO exposure
438 has been documented previously,[3, 6, 52, 53, 54] the critical insight obtained here is that DM*^{DAMGO}
439 heterodimers, despite their very low fraction (9.1% of M*^{DAMGO} at low physiological expression
440 levels of ≈1+1 copies/μm^2 of MOR and DOR) and short lifetime (369 ± 11 ms; Fig. 6c, d),
441 contribute to a significant proportion of M*^{DAMGO} internalization.

442 These observations suggest an unanticipated regulatory mechanism for M*^{DAMGO}
443 internalization. Namely, at the moment of DM*^{DAMGO} heterodimer formation, its ability to bind
444 to cellular internalization machineries, such as GRKs and β-arrestin 2,[55] might suddenly rise
445 dramatically, and then the binding affinity would rapidly decline due to DM*^{DAMGO} heterodimer
446 dissociation, which would occur within a fraction of a second ($1/k_{off}$ = 0.37 s; Supplementary
447 Table 3). Hence, the cycle of DM*^{DAMGO} heterodimerization and dissociation (which occurs every
448 few seconds or so) would function analogously to a car driver adjusting the speed by frequently
449 and briefly pushing on and releasing the gas pedal, to regulate the M*^{DAMGO} internalization rate
450 (Fig. 8c). Although the enhancement of internalization might occur only during the brief periods
451 when DM*^{DAMGO} heterodimers are formed (Fig. 8c), the total frequency of heterodimerization
452 across the PM ensures that the overall internalization of M*^{DAMGO} as DM*^{DAMGO} heterodimers is
453 significant. This correlates with the area under the curve consisting of many short pulses,
454 depicted in Fig. 8c.[56, 57, 58] Thus, the overall internalization rate of M*^{DAMGO} could be modulated
455 by the frequencies and durations of transient DM*^{DAMGO} heterodimerization events.

456 M*^{DAMGO} monomer/homodimer internalization would occur much less efficiently at the
457 level of individual molecules, but since larger fractions of M*^{DAMGO} exist as monomers at any
458 moment, the overall contributions of M*^{DAMGO} monomers/homodimers to M*^{DAMGO}

459 internalization are quite significant (Fig. 8c). If the expression levels of MOR and DOR are
460 elevated in certain cell types, then M^{*DAMGO} internalization would predominantly occur through
461 DM^{*DAMGO} heterodimers.

462 We also examined the effects of the DOR-specific agonist SNC-80 on receptor
463 internalization.[59] The treatment led to extensive internalization of SNC-80-bound DOR (D^{*SNC})
464 in both D- and MD-cells, with similar extents and rates (Supplementary Fig. 6a, middle and
465 right columns; Supplementary Table 5), indicating that DOR^{*SNC} is internalized without the
466 influence of heterodimerization with MOR. Meanwhile, SNC-80 induced significant MOR
467 internalization in MD-cells, which was reduced by the further addition of Dpep(20-42)DM
468 (Supplementary Fig. 6a, left column; Supplementary Table 5), indicating that MOR is
469 internalized when it forms heterodimers with D^{*SNC} in MD-cells.

470

471 **Transient DM^{*Ago} heterodimers produce strong short pulse-like signals**

472 We examined the cytoplasmic signals triggered by M-agonists, morphine and DAMGO, by
473 monitoring the intracellular Ca^{2+} mobilization in cells stably expressing Gqi5 and MOR, which
474 were further transiently transfected to express DOR or KOR (called M-, MD-, and MK-cells in
475 this subsection; Fig. 8d; cf Supplementary Fig. 1a and Methods as well as the caption to
476 Supplementary Fig. 1a in the companion paper). All ORs were expressed at the same low
477 physiological expression levels employed for single-molecule detection of dimers (0.5-1.0
478 fluorescent spots/μm^2 for each OR).

479 In M-cells, Ca^{2+} mobilization occurred at comparable intensities upon morphine and
480 DAMGO treatments, without any effect of Dpep(20-42)DM (in the companion paper, which also
481 reports Ca^{2+} mobilization in M-cells, we only used DAMGO as an MOR agonist). No response
482 was evident in D-cells or K-cells (only DAMGO was examined for K-cells). In MD-cells,
483 augmentations of the Ca^{2+} signal compared to that in M-cells were apparent for both morphine
484 and DAMGO (Ca^{2+} signal increase in MD-cells was greater with DAMGO than morphine), which
485 were mitigated by Dpep(20-42)DM. These observations indicate that the overall M^{*Ago}

486 downstream signals (M^{*Ago} denotes agonist-bound MOR, collectively indicating M^{*mor} and
487 M^{*DAMGO}) are greater when DOR is co-expressed. This result is consistent with a previous report
488 indicating that morphine and DAMGO activate MOR with greater efficacy when DOR is co-
489 expressed over MOR alone, but without explicitly estimating the percentages of MOR existing
490 as DM heterodimers.[50]

491 We found very small fractions of M^{*Ago} molecules existing as DM^{*Ago} heterodimers (4.9%
492 for DM^{*mor} and 9.1% for DM^{*DAMGO} at low experimental expression levels of ≈1+1 copies/μm^2
493 in Supplementary Table 3) for very brief durations (369 ± 11 ms for DM^{*DAMGO} and 187 ± 20
494 ms for DM^{*mor}; Fig. 6c). In the case of DAMGO, M^{*DAMGO} molecules existing as a *homo*dimer
495 induce the same signal level as M^{*DAMGO} existing as a monomer (since the presence of FAM-
496 Mpep-TAT or mGFP-Mpep does not affect the Ca^{2+} signal level; Figure 6F in companion paper).
497 These results suggest that the signal production rate (signal induced per unit time) of each
498 M^{*Ago} molecule in a DM^{*Ago} heterodimer must be substantially larger than that of each
499 monomeric or homodimeric M^{*Ago} molecule. This enhanced signaling rate may be induced by
500 conformational changes of M^{*Ago} upon DOR binding and/or those of DOR upon M^{*Ago} binding,
501 which might make a non-ligated DOR signal possible.

502 The enhanced signal from the M^{*Ago} molecules in very limited populations of DM^{*Ago}
503 heterodimers existing for short periods (369 ms) suggests a fundamentally important signaling
504 mechanism by DM^{*Ago} heterodimers, for the same reasons as the enhanced internalization upon
505 DM^{*DAMGO} heterodimerization (previous subsection). Namely, at the moment of DM^{*Ago}
506 heterodimer formation, the probability that the M^{*Ago} molecule and possibly the M^{*Ago}-bound
507 DOR molecule bind to and activate Gqi5 or Gαi, consequently triggering downstream signaling
508 cascades, might rise steeply, but this activation is short-lived because the DM^{*Ago} heterodimer
509 dissociates quickly within fractions of a second ($1/k_{off}$ = 0.19 s and 0.37 s for DM^{*mor} and
510 DM^{*DAMGO}, respectively; Supplementary Table 3). Hence, a DM^{*Ago} heterodimer will create brief,
511 pulse-like signals, and thus the signal in the entire cell is produced as the sum of the brief,
512 stronger pulse-like signals from individual DM^{*Ago} heterodimers plus the weaker signals from

513 M*^{Ago} monomers (Fig. 8c).[56, 57, 58] As we proposed previously,[56, 57, 58] the regulation of the signal
514 time courses of an entire cell is more readily achieved when signaling entities (individual
515 signaling molecules and molecular complexes) emit short pulse-like signals as opposed to
516 prolonged ones: only simple summation (aggregation) of brief signals suffices to generate the
517 overall cellular signal response, while if individual signals are prolonged, complex integration
518 rather than simple summation must be performed to produce the required cellular signal time
519 courses.[58] In short, the cellular signal intensities might be regulated by adjusting the
520 frequencies of the short pulse-like formation of DM*^{Ago} heterodimers. In addition, in cells with
521 elevated but still physiological OR expression levels, the signals emanating from DM*^{Ago}
522 heterodimers could be quite substantial, governing the cellular signal.
523

524 **Dpep(20-42) reduces morphine tolerance in mice**

525 As described in the previous subsection, Dpep(20-42)DM moderately reduces the M*^{Ago}-
526 induced signal. This effect not only has implications at the cellular level but also might extend
527 to broader physiological contexts, including nervous tissues and systemic functions. Therefore,
528 we examined whether the soluble DM heterodimer blocker peptide Dpep(20-42)DM can
529 modulate morphine-mediated analgesia in murine models. The peptide, dissolved in artificial
530 cerebrospinal fluid (aCSF), was administered directly into the cerebral ventricles at a dose of
531 10 μg/day continuously for two days prior to the commencement of daily subcutaneous
532 morphine injections (10 mg/kg/injection; one injection/day) (Fig. 8f). We utilized the tail-flick
533 test to evaluate the analgesic efficacy of morphine and track the progression of antinociceptive
534 tolerance.

535 Our results revealed that the analgesic potency of morphine was enhanced by Dpep(20-
536 42)DM, which was especially evident between 60 and 120 minutes after morphine application
537 over the course of the study (days 1, 5, 8, and 11; Supplementary Fig. 6b). Notably, on day
538 11, the disparity in analgesic effects between the control aCSF and the peptide groups reached
539 ≈3 fold at the 120-minute mark following morphine administration (Fig. 8g).

540 Furthermore, the administration of Dpep(20-42)DM reduced the development of morphine
541 tolerance. By day 8 after the morphine treatment was initiated, a noticeable reduction in
542 morphine's analgesic effect was observed in the control group. In contrast, mice treated with
543 the peptide retained ≈80% of the initial antinociceptive efficacy, which was sustained from
544 days 8 to 11 (Fig. 8h). These results imply that the inhibition of DM* heterodimerization by
545 Dpep(20-42)DM diminishes the development of antinociceptive tolerance to morphine,
546 suggesting the involvement of crucial neuronal populations within the pain pathway that co-
547 express MOR and DOR, corroborating prior studies.[3, 18, 21, 24] Suppression of DM* heterodimers
548 by Dpep(20-42)DM also diminishes the cellular signal levels (Fig. 8e). Accordingly, maintaining
549 proper signal levels in cells might be important for sustained morphine analgesia, which will be
550 discussed further.

551 # Discussion

552 The significance of OR heterodimerization in pain therapy and neuropsychiatric disorders is
553 garnering increasing attention.[7, 8, 9, 10] However, our understanding of OR heterodimers and
554 their clinical implications is limited due to the paucity of fundamental knowledge on heterodimer
555 formation dynamics and mechanisms and the lack of specific blockers. Using our advanced
556 single-molecule imaging and analysis methods,[1] we obtained the fundamental parameters K_D,
557 k_{off}, and k_{on}, describing OR homo- and hetero-dimerizations. Crucially, these parameters are
558 independent of OR expression levels, and thus we firmly established the formation of transient
559 DM and DK heterodimers, alongside KK, MM, and DD homodimers, in the PM of cells expressing
560 these molecules. These parameters were determined in the presence and absence of M-
561 agonists and Dpep(20-42)DM (Fig. 6e and Supplementary Tables 2-3), and the percentages of
562 protomers existing as DM and DK heterodimers at various expression levels were calculated
563 from the K_D values (Supplementary Tables 3-4 and Supplementary Fig. 5), which will be useful
564 for future studies to reveal the biological and pharmacological consequences of OR homo- and
565 hetero-dimers. We hardly detected transient OR trimers and tetramers, indicating that at low
566 physiological expression levels, the percentage of OR protomers existing as oligomers greater
567 than dimers would be limited.

568 This study first documented the transient nature of OR heterodimers, revealing lifetimes
569 of DM and DK heterodimers of approximately 250 ms, roughly twice as long as those of
570 homodimers (120 ms for DD and MM and 180 ms for KK). Previous single-molecule imaging
571 studies likely missed the OR dimers due to their scarce presence at the low expression levels
572 typically employed in these studies (≈1 copy/μm^2) and their brief lifetimes.[60, 61, 62] Indeed,
573 experiments performed at higher protein densities using bioluminescence resonance energy
574 transfer (BRET), fluorescence resonance energy transfer (FRET), and biochemical assays
575 detected the dimers, although these methods could not elucidate the dynamic nature of OR
576 dimerization.[44, 61, 63, 64, 65] Interestingly, pull-down assays, which require minute-order

577 procedures, detected homo- and hetero-dimers despite their 100-ms-order lifetimes,[18, 66]
578 probably due to the rapid reassociation kinetics.

579 The interaction domains critical for heterodimerization have been identified as both the
580 N-terminal domains for DM and both the EL3 domains for DK heterodimers (Fig. 2-4). While
581 TM domains contribute to dimerization, they are less specific and primarily augment overall
582 affinity. For example, $TM1^{MOR}$ is involved in MM *homo*dimerization by binding to another MOR
583 (perhaps mainly the TM1 domain), in addition to DM *hetero*dimerization by binding to $TM1^{DOR}$,
584 $TM4^{DOR}$, and other TMs of DOR (Fig. 5b-d). The nature of lower-specificity TM interactions is
585 also found in the literature. The involvement of TM domains in DM heterodimerization[3, 46] and
586 DK heterodimerization was previously proposed,[31] whereas the same TM domains such as
587 $TM4^{DOR}$ and $TM1^{MOR}$ were also proposed to be involved in DD[67] and MM[48, 68] homodimerizations.
588 As described in the companion paper, specific C-terminal interactions are critical for the
589 formation of KK, MM, and DD homodimers. The TM interactions with lower specificities were
590 previously proposed as the rolling dimer interface model, in which multiple TM interaction sites
591 co-exist and interconvert.[44]

592 Since the addition of either Dpep(20-42)DM (also Mpep(32-61)MD) or $TM1^{MOR}$ alone
593 reduced the colocalization index for DM heterodimers to near-baseline levels (1.2-1.3) (Fig. 4a,
594 b, and 5c), we suggest that DM heterodimerization might also involve cooperative allosteric
595 conformational changes between the N-terminal domains and TM domains in DOR and MOR,
596 which might affect their functions.[69] In addition, although the binding of nucleotide-free Gα to
597 GPCR was proposed to affect GPCR conformations,[70] we did not consider this effect on OR
598 dimerization. The possible involvement of these processes suggests the complexity of OR
599 dimerization, which we have simplified using first-order kinetics to aid our understanding at this
600 stage of research.

601 Our findings also suggest that while TM peptides from ORs will not serve as specific
602 blockers for OR homo- and hetero-dimerizations (Fig. 5c and d),[3] soluble peptides with
603 sequences mirroring the extracellular heterodimer formation domains ($EL3^{DOR}$ and $EL3^{KOR}$

604 peptides for DK heterodimers and DpepDM and MpepMD for DM heterodimers) can specifically
605 reduce DM and DK *hetero*dimers (Fig. 2d, 4, and 5d).

606 We extensively utilized the Dpep(20-42)DM peptide to dissect the functions of M^{*Ago}
607 monomers/homodimers and DM^{*Ago} heterodimers after the application of M-agonists, morphine
608 and DAMGO (where M^{*Ago} collectively denotes agonist-bound MOR). DM^{*Ago} dimerization was
609 enhanced by DAMGO but not morphine, and reduced by Dpep(20-42)DM (Fig. 6). Morphine
610 does not induce the internalization of M^{*mor} or DOR even in MD-cells, where DM^{*mor}
611 heterodimerization is induced. M^{*DAMGO} monomers and $M^{*DAMGO}M^{*DAMGO}$ homodimers are
612 internalized in similar manners (Fig. 6b in the companion paper), and DM^{*DAMGO}
613 heterodimerization further enhanced M^{*DAMGO} internalization (Fig. 8b and c). DM^{*Ago}
614 heterodimerization also enhanced the downstream Ca^{2+} signal (Fig. 8e). Monomers of a
615 prototypical GPCR, the β2-adrenergic receptor, were previously found to efficiently activate a
616 stimulatory heterotrimeric G protein, Gs,[71] but our results indicate that certain GPCRs, including
617 MOR, might acquire enhanced activities upon heterodimer formation.

618 In our study, conducted under the low physiological receptor expression levels (≈1+1
619 copies/μm^2), only small fractions (≤9.1%) of M^{*Ago} will exist as DM^{*Ago} heterodimers at any
620 moment (Supplementary Table 3). Combining this with the short 369-ms lifetime of DM^{*Ago}
621 heterodimers, we advanced an argument that each DM^{*Ago} heterodimer will create a brief,
622 intense pulse-like signal, contrasted with the weaker signals from M^{*Ago} monomers, and the
623 overall cellular signal is produced as the sum of these signals (Fig. 8c, e).[56, 57, 58] Note that all
624 M^{*Ago} molecules form DM^{*Ago} heterodimers every 1-10 s even under lower normal physiological
625 expression levels (Fig. 6e and Supplementary Table 3). Enhanced internalization of M^{*DAMGO}
626 might also follow a similar enhancement pattern. These results were observed under expression
627 levels far lower than those typically used in bulk optical and biochemical assays (by factors of
628 10-1000),[63, 64, 65] suggesting a unique signaling mechanism in native physiological conditions.

629 In specific neural tissue domains or certain cell types where OR expression levels are
630 higher,[51] DM^{*Ago} heterodimers could play more dominant role in cellular responses, dictated by

631 the frequency of their transient active phases. Building upon this hypothesis, and recognizing
632 the possibility that small quantities of DM*^{Ago} heterodimers might induce critical signals in key
633 neurons, we explored the *in vivo* effects of Dpep(20-42)DM administered into murine cerebral
634 ventricles to assess its impact on morphine tolerance, unlike a previous study using systemically
635 applied Nterm-TM1^{MOR}-TAT,[3] which would non-specifically block multiple dimer forms (Fig. 5).
636 We found that cerebral ventricle-administered Dpep(20-42)DM significantly curtails the
637 development of long-term tolerance (Fig. 8f-h). However, directly comparing the effectiveness
638 of Dpep(20-42)DM to Nterm-TM1^{MOR}-TAT is challenging due to differing administration methods
639 and the inherent specificity of Dpep(20-42)DM, which likely contributes to its reduced side
640 effects.

641 Our *in vivo* findings align with previous findings that a genetic or pharmacological
642 blockade of DOR can enhance MOR-agonist induced analgesia, highlighting the role of DM
643 heterodimers in regulating MOR-mediated pain pathways[4, 18, 21, 24, 72, 73, 74] The newly identified
644 specific extramembrane domains identified for DM heterodimer-blocking present novel targets
645 for modulating OR function, offering strategic avenues for the development of opioid therapies
646 with reduced tolerance and dependence.

647 These *in vivo* results should be compared with our findings in cultured cells, where
648 Dpep(20-42)DM, facilitating DM*^{mor} dissociation into monomers, reduces the Ca^{2+} signal from
649 Gqi5 (Fig. 8e). These apparently contrasting findings made *in vivo* and *in vitro* suggest that
650 finely tuning cellular signals upon morphine application is crucial for preventing long-term
651 tolerance in mice. Agents that modulate the levels of DM*^{mor} heterodimers in the PM, like
652 Dpep(20-42)DM, could offer more precise control over drug effects than simply varying
653 morphine dosage.

654

Figures

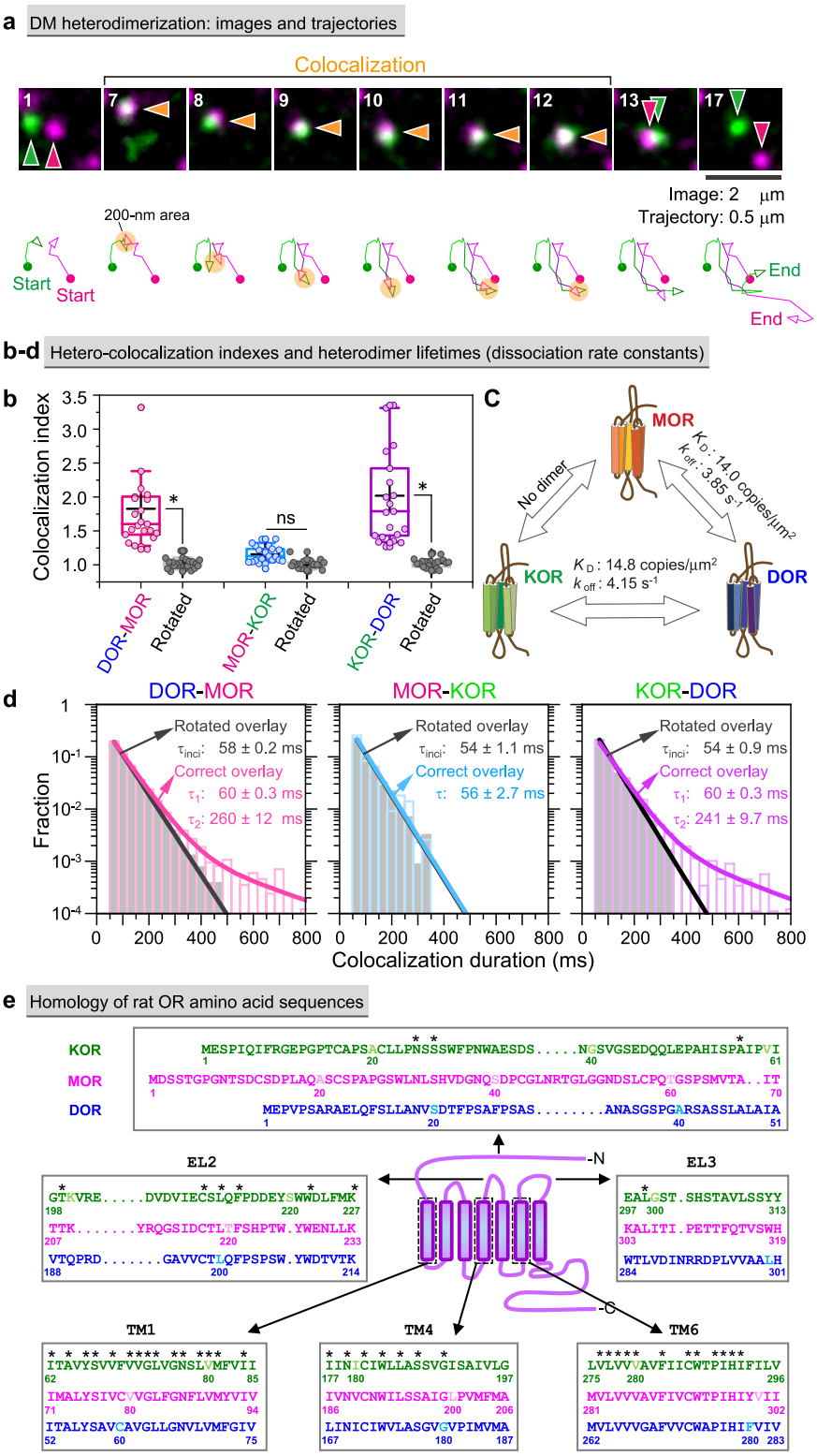

Fig. 1: Transient DM and DK heterodimers, but not MK heterodimers, form in the PM.

659 **a** Typical image sequence of simultaneous two-color single fluorescent molecule observations
660 and trajectories of the molecules shown in the images. These molecules undergo transient
661 hetero-colocalization and co-diffusion (SNAP-Surface 549-labeled SNAPf-DOR, green;
662 SaraFluor650T-labeled MOR-Halo, magenta).
663 **b** DM and DK heterodimers form, but MK heterodimers do not, as detected by colocalization
664 indexes for correct and rotated overlays (see Supplementary Fig. 2c-e in the companion paper.[1]
665 Throughout this report, we employ the following conventions. For box plots, horizontal
666 bars, crosses, boxes, and whiskers indicate the median values, mean values, interquartile
667 ranges (25-75%), and 10-90% ranges, respectively; for bar graphs and plots showing mean
668 values, SEM values are provided by bars; and in statistical analyses, * and ns (not significant)
669 indicate $p < 0.05$ and $p \geq 0.05$, respectively, obtained by Tukey's multiple comparison test.
670 The result set used for multiple comparison is indicated by the group of lines in each figure,
671 and different sets are indicated by different colors (e.g., Fig. 2c, 3c and 7e). All statistical
672 parameters (number of replicates and *p* values) are summarized in Supplementary Table 1.
673 **c** Summary of K_D and k_{off} values for OR heterodimers.
674 **d** Histograms showing the distributions of hetero-colocalization *durations* for correct and
675 rotated overlays. The control histograms for rotated overlays (grey) were fitted by single
676 exponential functions (black), providing the lifetimes of the incidental overlap events between
677 the magenta and green spots (τ_{inci}). The histograms for correct overlays (colors) were fitted by
678 the sum of two exponential functions: The faster decay time (τ_1) was close to the lifetime of
679 incidental overlaps (τ_{inci}), and the slower decay time provided the heterodimer lifetime (τ_2). The
680 heterodimer lifetime after correction for the trackable duration lifetime is shown in each box.
681 The k_{off} values ($1/\tau_2$) calculated from τ_2 are shown in **c**.
682 **e** Comparison of the amino acid sequences among the three classical ORs (rat) in the domains
683 where the amino acid homologies are lower. Asterisks mark the identical amino acids.

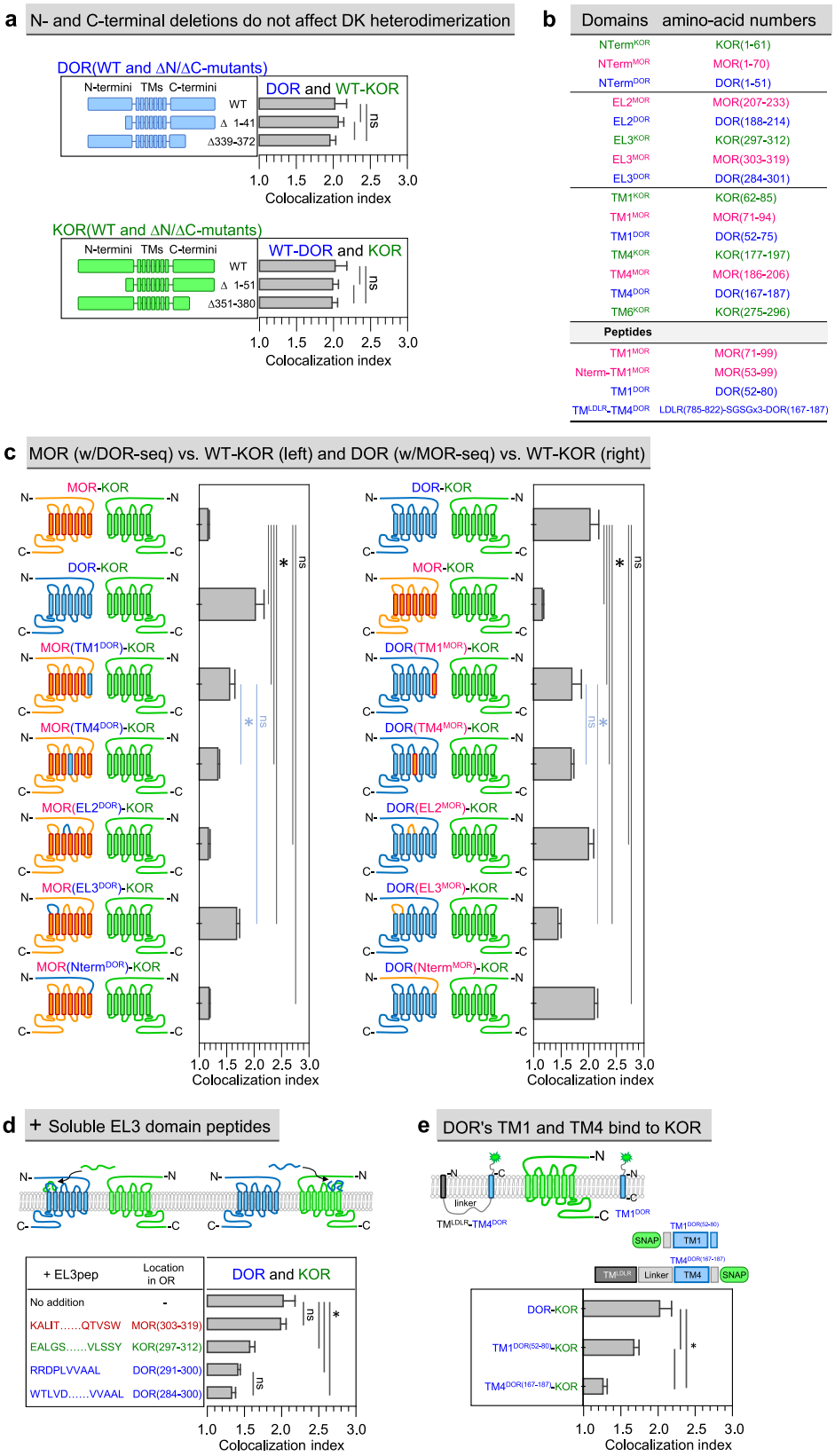

Fig. 2: Interaction between EL3 domains of DOR and KOR is involved in DK heterodimerization, and DOR's TM1 and TM4 are also involved.

687 **a** The N- and C-terminal domains of DOR and KOR are not involved in DK heterodimerization.
688 DK colocalization indexes of N/C-terminal deletion mutants of DOR and full-length KOR (top)
689 and N/C-terminal deletion mutants of KOR and full-length DOR (bottom).
690 **b** Summary of the names and exact amino-acid ranges of the OR domains and TM1-based
691 peptides employed in this work.
692 **c** DOR's EL3, TM1, and TM4, but not EL2 and N-term, are involved in DK heterodimerization.
693 (Left panel) Because MK heterodimerization scarcely occurs (top), we examined whether MK
694 heterodimerization (MK colocalization index) is enhanced by substituting various MOR domains
695 with the corresponding DOR domains, using WT-KOR as the binding partner (DK
696 heterodimerization as a positive control; second). (Right panel) Because DOR binds to KOR to
697 form DK heterodimers (top) and MK heterodimerization rarely occurs (second), we examined
698 whether DK heterodimerization (DK colocalization index) is reduced by substituting various DOR
699 domains with the corresponding MOR domains, using WT-KOR as the binding partner.
700 **d** Both EL3 domains of DOR and KOR are involved in DK heterodimerization. Soluble peptides
701 (1 μM) with the aa sequences of the EL3 domains (EL3-domain peptides) of DOR and KOR, but
702 not that of MOR, block DK heterodimerization.
703 **e** DOR's TM1 and TM4 bind to KOR. Colocalization indexes show that the affinities to WT-KOR
704 are greater in the order of WT-DOR > DOR's TM1 > DOR's TM4.
705

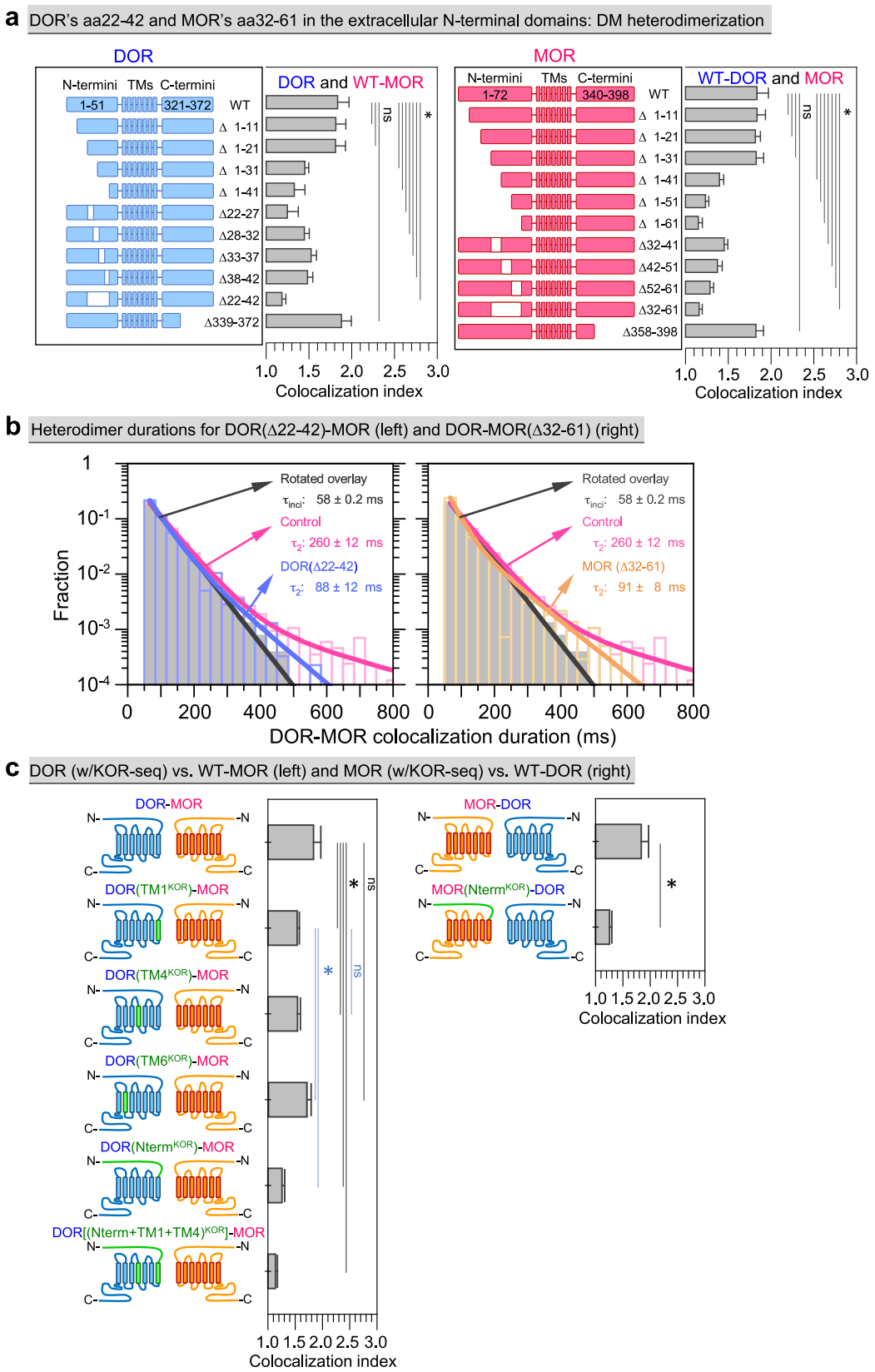

Fig. 3: N-terminal domains of DOR's aa22-42 and MOR's aa32-61, as well as DOR's TM1 and TM4 domains, are involved in DM heterodimerization.

709 **a** Involvement of the extracellular N-terminal domains of DOR and MOR in DM
710 heterodimerization, particularly that of DOR's aa22-42 and MOR's aa32-61. The figures show
711 that mutants with various deletions in the N-terminal domains of DOR and MOR exhibit lower
712 colocalization indexes with full-length (WT) MOR and DOR, respectively, compared to the
713 colocalization index between full-length DOR and MOR. At the bottoms of both panels are the
714 results for the C-terminal deletion mutants, indicating the lack of cytoplasmic C-terminal domain
715 involvement in DM heterodimerization.
716 **b** Histograms showing the colocalization *duration* distributions for the pair of WT-MOR and
717 DOR(Δ22-42) (left, blue) and the pair of WT-DOR and MOR(Δ32-61) (right, magenta).
718 Histograms for the control and rotated overlays of WT DOR-MOR images are the same as those
719 shown in **Fig. 1d.**
720 **c** The extracellular N-terminal domains of DOR and MOR are involved in DM heterodimerization
721 (left and right panels, respectively), as are DOR's TM1 and TM4 domains, but not the TM6
722 domain (left panel). (Left panel) Based on the finding that MK heterodimerization hardly occurs,
723 we examined whether the DM colocalization index is reduced upon substitutions of DOR
724 domains with the corresponding KOR domains, using WT-MOR as the partner. (Right panel)
725 The DM colocalization index is reduced upon the substitution of MOR's N-terminal domain with
726 KOR's N-terminal domain, which is not involved in DK heterodimerization (Fig. 2a), indicating
727 the involvement of MOR's N-terminal domain in DM heterodimerization.
728

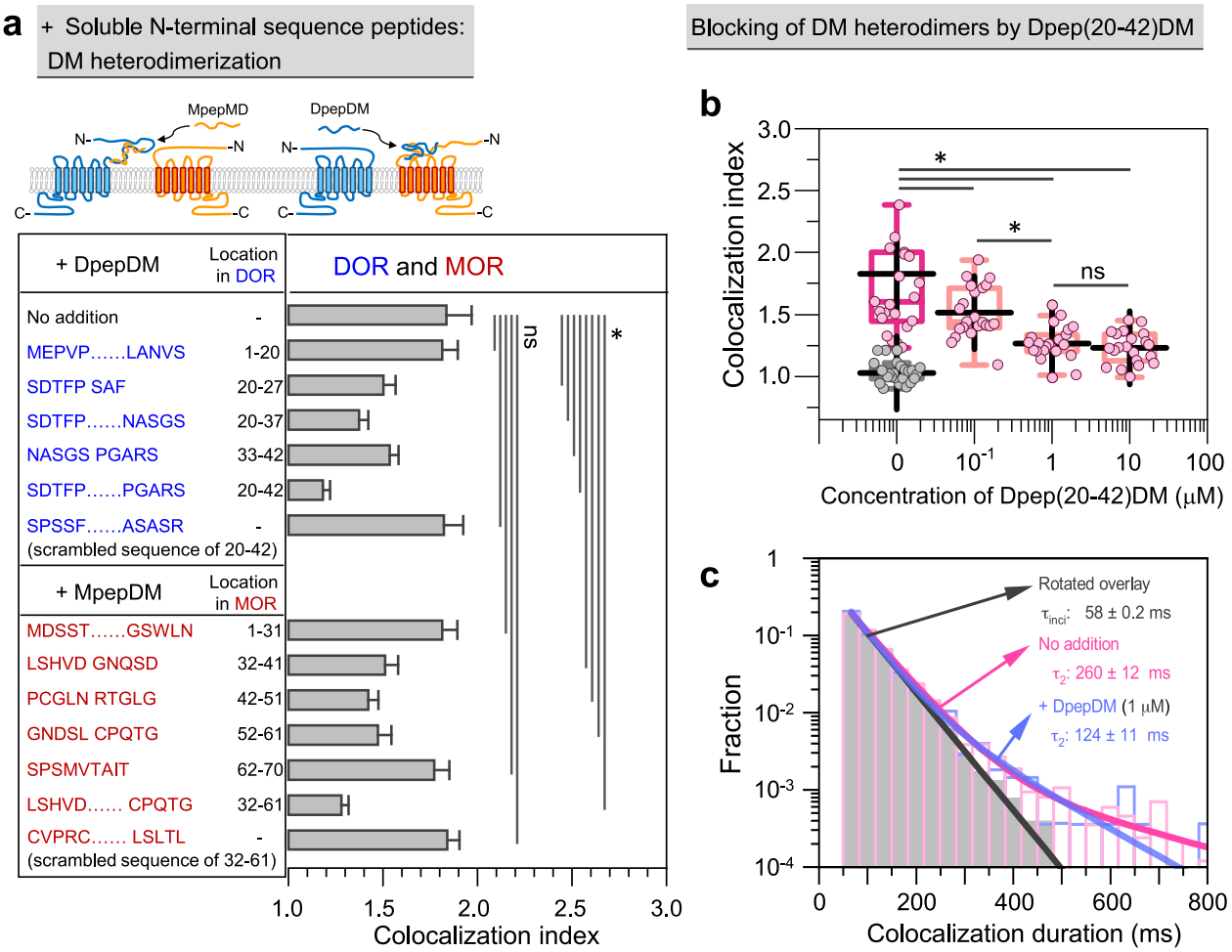

Fig. 4: Soluble Dpep(20-42)DM and Mpep(32-61)DM peptides suppress DM heterodimerization.

a Effect of the addition of 1 μM soluble peptides with the same amino-acid sequences as various parts of the N-terminal domains of DOR and MOR (DpepDM and MpepDM, respectively) on the DM colocalization index.

b With an increase of the Dpep(20-42)DM concentration, the DM colocalization index decreased. The grey keys at 0 μM Dpep(20-42)DM represent the data points obtained by using rotated overlays.

c Dpep(20-42)DM reduces the τ_2 of DM colocalization (blue). Histograms for the control (no addition) and rotated overlays of WT DOR-MOR images are the same as those shown in **Fig. 1d.**

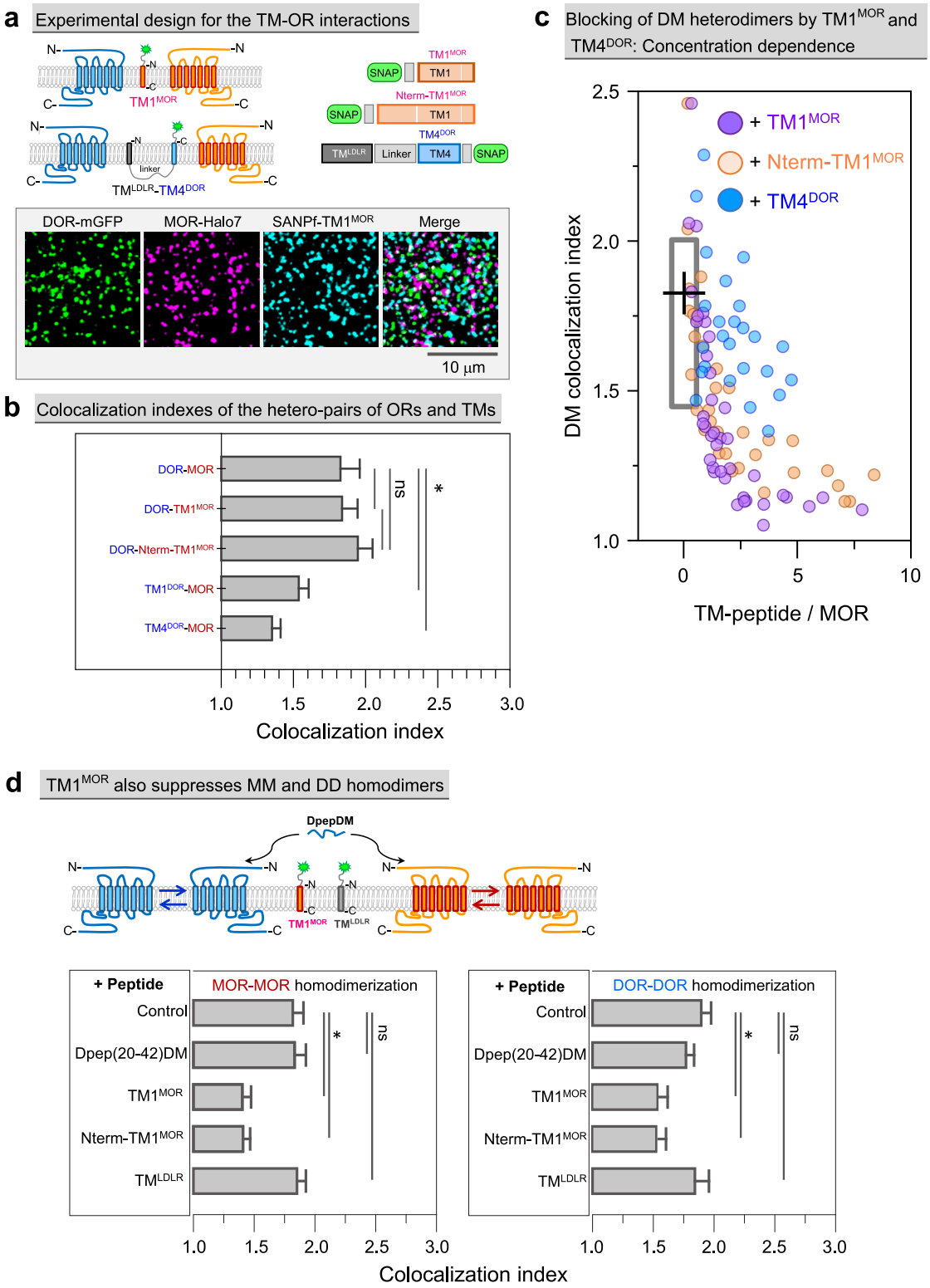

Fig. 5: TM1^{MOR} interacts with DOR and blocks DM heterodimers, and additionally inhibits MM and DD homodimers, whereas Dpep(20-42)DM only blocks DM heterodimer formation.

746 **a** Experimental design for examining the interactions of $TM1^{MOR}$, Nterm-$TM1^{MOR}$, and $TM4^{DOR}$
747 (Fig. 2b) with WT-ORs (top). For the correct orientation of $TM4^{DOR}$ in the PM, it was linked to
748 the transmembrane domain of LDL receptor (TM^{LDLR}).[75] Representative single-molecule images
749 of DOR-mGFP (green), MOR-Halo (magenta), and SNAPf-$TM1^{MOR}$ (cyan) co-expressed at similar
750 levels of 0.5-1.0 fluorescent spots/μm^2 (bottom).
751 **b** $TM1^{MOR}$ and Nterm-$TM1^{MOR}$ form dimers with WT-DOR as efficiently as WT-MOR does. $TM1^{DOR}$
752 and $TM4^{DOR}$ form dimers with WT-MOR to lesser extents. Expression levels of all molecules
753 were adjusted to 0.5-1.0 fluorescent spots/μm^2.
754 **c** Reduction of the DM colocalization index with an increase in the number densities of the TM
755 peptides ($TM1^{MOR}$, Nterm-$TM1^{MOR}$, and $TM4^{DOR}$) relative to that of MOR, expressed in the PM.
756 DOR and MOR were both expressed at levels of 0.5-1.0 fluorescent spots/μm^2. The effects of
757 $TM1^{MOR}$ and Nterm-$TM1^{MOR}$ are stronger than that of $TM4^{DOR}$. The rectangular box without the
758 peptides (x = 0) indicates the result of the box plot without datapoints (to avoid excessive
759 complexity in the plot).
760 **d** $TM1^{MOR}$ and Nterm-$TM1^{MOR}$ reduce MM and DD homodimers (in addition to DM
761 heterodimers), but 1 μM Dpep(20-42)DM does not. $TM1^{MOR}$ and Nterm-$TM1^{MOR}$ expression
762 levels were ≈10x of MOR and DOR, following the results shown in panel **c**. TM^{LDLR} is a
763 negative control, representing non-interacting TM domains.
764

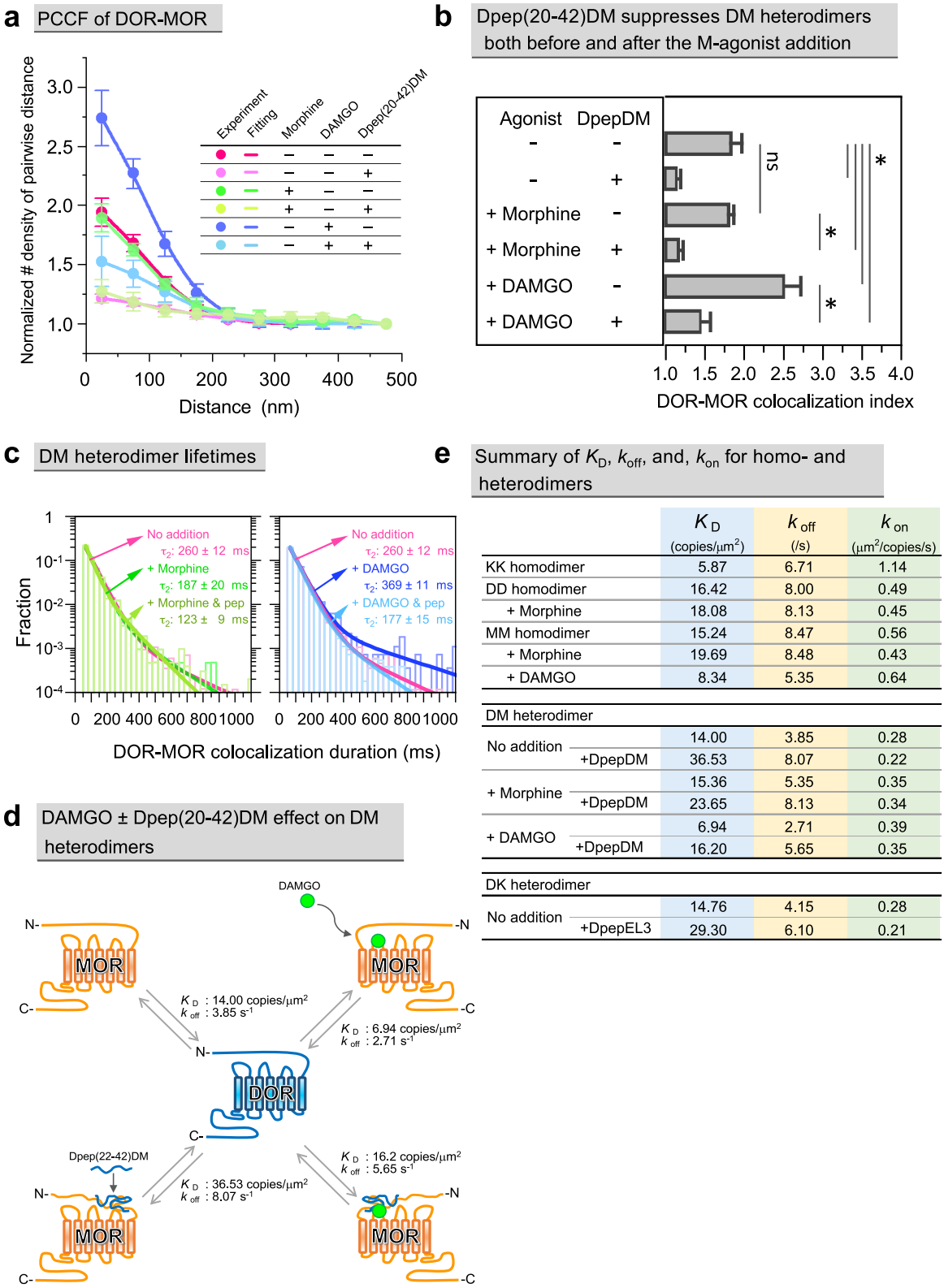

		K_D (copies/μm^2)	k_{off} (/s)	k_{on} (μm^2/copies/s)
KK homodimer		5.87	6.71	1.14
DD homodimer		16.42	8.00	0.49
+ Morphine		18.08	8.13	0.45
MM homodimer		15.24	8.47	0.56
+ Morphine		19.69	8.48	0.43
+ DAMGO		8.34	5.35	0.64
DM heterodimer				
No addition		14.00	3.85	0.28
	+DpepDM	36.53	8.07	0.22
+ Morphine		15.36	5.35	0.35
	+DpepDM	23.65	8.13	0.34
+ DAMGO		6.94	2.71	0.39
	+DpepDM	16.20	5.65	0.35
DK heterodimer				
No addition		14.76	4.15	0.28
	+DpepEL3	29.30	6.10	0.21

Fig. 6: Effects of M-agonists, morphine and DAMGO, on DM heterodimerization, and of Dpep(20-42)DM on DM heterodimerization, in the presence of M-agonists.

768 **a** Experimental PCCFs for DM heterodimerization in the presence and absence of 0.5 μM M-
769 agonists and 1 μM Dpep(20-42)DM and their fitting curves using K_D for DM heterodimerization
770 and σ (precisions of single-molecule localizations for the two probes and spatial precision for
771 overlaying two-color images) as fitting parameters. MD-cells expressing both DOR and MOR at
772 0.5-1.0 fluorescent spots/μm^2 were employed.
773 **b** Colocalization indexes obtained from the PCCFs shown in **a**. Together with the results shown
774 in **a**, the results indicate that morphine hardly affects DM heterodimerization whereas DMAGO
775 enhances it. The Dpep(20-42)DM addition significantly reduces DM heterodimers under all
776 conditions examined here.
777 **c** Morphine shortens and DAMGO prolongs DM heterodimer lifetimes, whereas the further
778 addition of Dpep(20-42)DM reduces the lifetimes, making them shorter than those for DM
779 heterodimers without any treatment.
780 **d** Schematic summary of K_D and k_{off} values for DM heterodimers in the presence and absence
781 of DAMGO and DpepDM(20-42)DM.
782 **e** Summary of K_D, k_{off}, and k_{on} values for OR homodimers and DM and DK heterodimers,
783 including the cases in the presence and absence of morphine or DAMGO and DpepDM(20-
784 42)DM (DpepEL3 in the case of DK heterodimers), wherever appropriate.
785

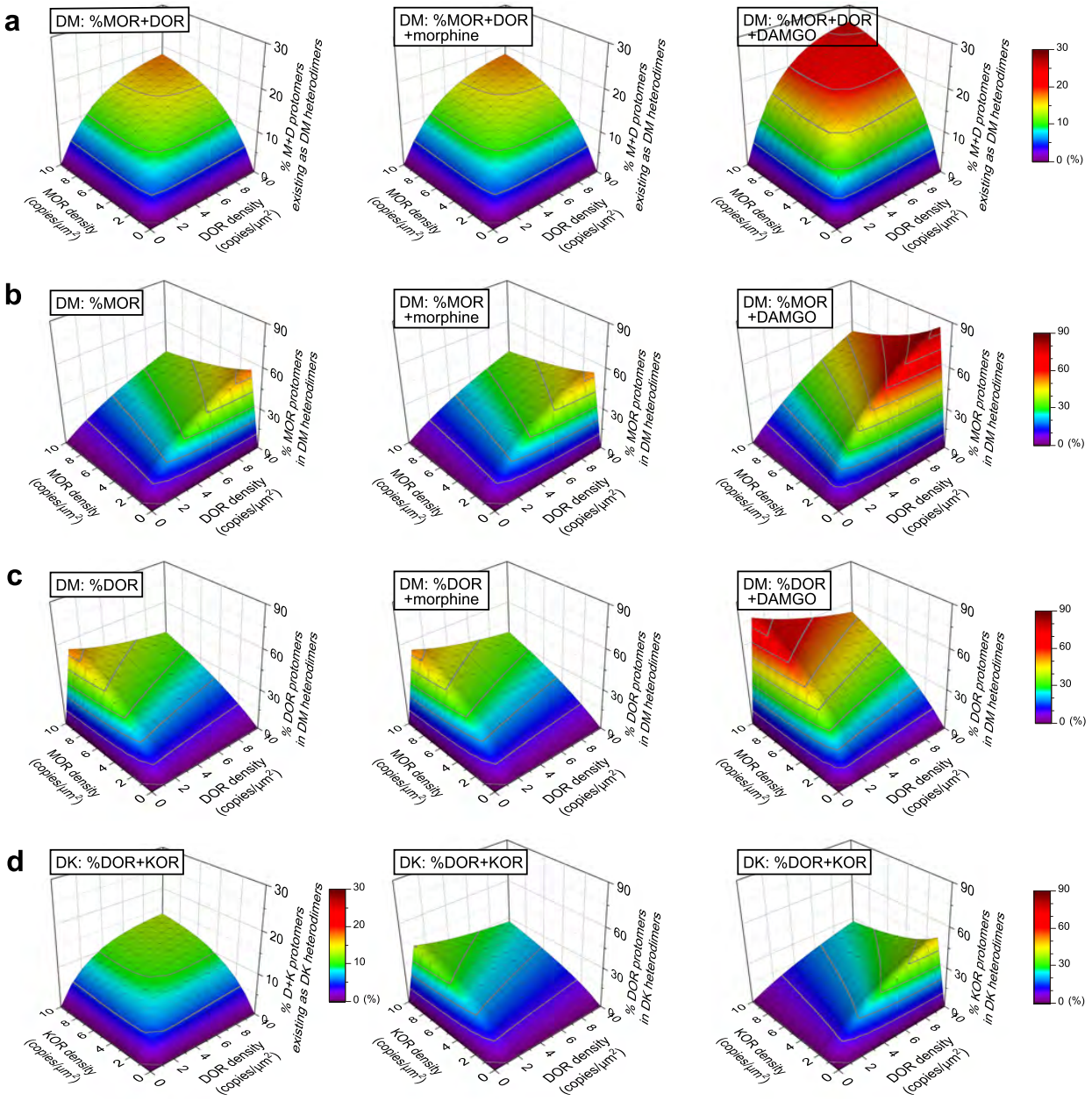

Fig. 7. The percentages of OR protomers existing as OR heterodimers at various expression levels (z-axis), predicted from the K_D values for homo- and hetero-dimer dissociation equilibrium.

In a-c, from left to right, no addition, + morphine, and + DAMGO.

a Overall percentages of MOR and DOR protomers existing as DM heterodimers.

b Percentages of MOR protomers existing as DM heterodimers.

c Percentages of DOR protomers existing as DM heterodimers.

794 **d** Overall percentages of DOR and KOR protomers existing as DK heterodimers (left),
795 percentages of DOR protomers existing as DK heterodimers (middle), and percentages of
796 KOR protomers existing as DK heterodimers (right).
797

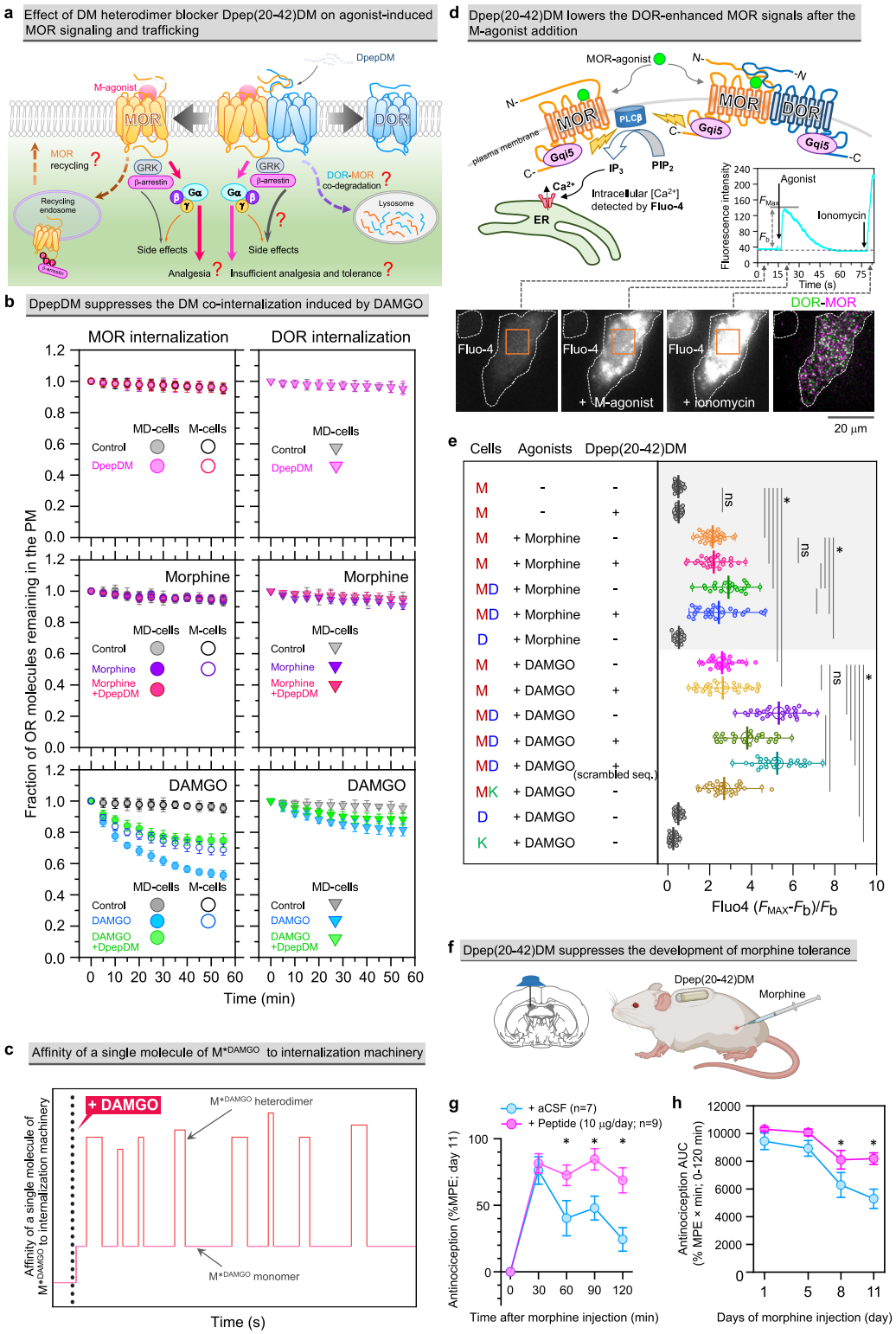

Fig. 8: Dpep(20-42)DM helps to dissect the DM heterodimer and MOR monomer functions after M-agonist applications in cells, and enhances morphine analgesia and reduces tolerance development in mice.

802 **a** Schematic figure showing that Dpep(20-42)DM reduces DM heterodimers, helping to dissect
803 the DM heterodimer and MOR monomer functions, including signaling and internalization, upon
804 M-agonist addition.
805 **b** Time courses of MOR and DOR internalization (left and right columns, respectively) before
806 and after the addition of 0.5 μM morphine or DAMGO (top, middle, and bottom boxes,
807 respectively) in the presence and absence of 1 μM DpepDM. MOR internalization was examined
808 in MD-cells and M-cells, whereas DOR internalization was observed only in MD-cells (MOR and
809 DOR internalizations upon D-agonist addition were observed in MD-cells and D-cells, see
810 Supplementary Fig. 6a). The fitting results for these time courses are not depicted here for
811 clarity, but are shown in Supplementary Fig. 5.
812 **c** Schematic illustration showing immensely enhanced efficiencies of binding to internalization
813 machineries such as GRKs and β-arrestins and of DM^{*DAMGO} heterodimer internalization,
814 occurring in the brief lifetimes of DM^{*DAMGO} heterodimers. M^{*DAMGO} monomers' internalization
815 efficiency is low, but due to the presence of many M^{*DAMGO} monomers, they are responsible for
816 the internalization of half of the M^{*DAMGO} molecules in the PM.
817 **d** (Top) Experimental design for observing Ca^{2+} mobilization after M-agonist addition. Ca^{2+}
818 mobilization was monitored by Fluo-4 fluorescence intensity in M-, D-, and MD-cells. (Bottom)
819 Fluo-4 images and single-molecule images of DOR and MOR. Ca^{2+} mobilization was
820 parametrized by using $[F_{Max}-F_b]/F_b$, where F_{Max} is the maximal Fluo-4 signal intensity within 75
821 s after stimulant addition and F_b is the baseline intensity (insert in Fig. d).
822 **e** Ca^{2+} mobilization parametrized by using $[F_{Max}-F_b]/F_b$ for Fluo-4 signals before and after the
823 addition of morphine and DAMGO, in the presence and absence of Dpep(20-42)DM.
824 **f** Schematic illustration showing the osmotic pump implantation for intracerebroventricular
825 injection of Dpep(20-42)DM and subcutaneous morphine injection in mouse.
826 **g** Tail flick test results on day 11, showing that morphine-induced analgesia was enhanced by
827 the continuous administration of Dpep(20-42)DM (10 μg/day). The enhancing effect lasted for
828 at least 120 min.

829 **h** Tolerance to morphine was demonstrated by the loss of the analgesic response from day 8,
830 reduced to ≈50% of the initial efficacy on day 11 in the control aCSF-treated mice (AUC = area
831 under the antinociception vs. time curves shown in Supplementary Fig. 6b). In contrast, the
832 antinociceptive effect of morphine in DpepDM-treated mice was maintained at ≈80% of the
833 initial efficacy on days 8 and 11. All experiments were randomized and performed by a blinded
834 researcher, who was then unblinded before statistical analysis.

835

836

837 # Methods

838 **cDNA construction**

839 See the companion paper under the same title.[1]

840

841 **Mice**

842 Male C57BL/6N mice (30-40 g) were purchased from CLEA Japan, Inc. and maintained on a
843 12-h light/dark cycle with rodent chow and water available ad libitum. They were housed in
844 groups of four until testing. Animal studies were performed according to protocols approved
845 by the Nagasaki University Animal Care and Use Committee (Approved number:
846 2002181596).

847

848 **Cell culture, transfection, and microscope observations**

849 See the companion paper under the same title.[1]

850

851 **Fluorescence labeling of ORs**

852 The SNAPf-tag-protein fused to ORs was fluorescently labeled with the SNAP-Surface 549
853 ligand, basically as described in the companion paper.[1] The Halo7-tag protein fused to the
854 intracellular C-terminus of the OR (Supplementary Fig. 1a) was covalently conjugated with
855 SaraFluor650T-Halo-ligand (Goryo Kayaku), by incubating the cells with 100 nM Halo ligand.
856 The SNAPf-OR and OR-Halo7 proteins were simultaneously labeled in the growth medium, at
857 37°C in the CO_2 incubator for 30 min. The cells were washed three times with fresh medium
858 (5-min incubation each time), and then the Ham's F12 observation medium was added.

859 The labeling efficiency was determined by using the SNAPf-CD47-mGFP and mGFP-
860 CD47-Halo7 proteins expressed in the PM (Supplementary Fig. 1c). CD47 is a monomeric 5-
861 pass transmembrane protein expressed in the PM.[76] We could not use ORs for this purpose
862 because they form transient dimers, and thus employed monomeric CD47. For further details,
863 refer to Methods and Supplementary Fig. 1c-e in the companion paper.[1]

The fluorescence labeling efficiencies under our normal conditions were 60% and 88% for SNAP-Surface 549 and SaraFluor650T, respectively (Supplementary Fig. 1c). By controlling the expression levels and using these labeling conditions, the spot numbers of SNAPf-OR and OR-Halo7 proteins were approximately equalized (0.75 ± 0.25 spots/μm^2 for each color; i.e., a total spot number density of 1.5 ± 0.5 spots/μm^2).

Single fluorescent-molecule imaging

Fluorescently labeled ORs expressed in the bottom PM (the PM facing the coverslip) at fluorescent-spot number densities of 0.75 ± 0.25 spots/μm^2 for each color (a total spot number density of 1.5 ± 0.5 spots/μm^2) were observed at the level of single molecules at 37°C, using a home-built objective lens-type TIRF microscope constructed on an inverted microscope (Olympus IX-83) (see the companion paper for details).[77, 78, 79] ORs tagged with fluorescent probes were excited with TIR illumination using the following power densities: SNAP-Surface 549 at 561 nm (Coherent OBIS 561-100 LS) at 0.35 $\mu W/\mu m^2$; and SaraFluor650T at 642 nm (Omicron LuxXPlus 640-140) at 0.50 $\mu W/\mu m^2$. Simultaneous two-color single-molecule imaging and analysis were conducted as described in the companion paper.[79]

Evaluating colocalization durations

See the companion paper under the same title. The trackable duration lifetime (τ_{track}) for SNAP-Surface 549 bound to SNAPf-MOR was 16.3 ± 1.2 s (n = 500; the same as those described in the companion paper) and that for SaraFluor650T-Halo-ligand bound to MOR-Halo was 12.5 ± 0.8 s (n = 500) (expressed in CHO-K1 cells) (Supplementary Fig. 1f).

Evaluating the colocalization index

See the companion paper under the same title.[1]

891 **Monte-Carlo simulations**

892 See the companion paper under the same title.[1]

893

894 **Cell treatments with agonists and peptides**

895 M-agonists, DAMGO (Sigma-Aldrich) and morphine (Takeda), and D-agonist SNC-80 (Sigma-
896 Aldrich) were applied to the cells as described in the companion paper. DpepDM and MpepMD
897 peptides, custom-synthesized by Cosmo-Bio, are soluble peptides, and were dissolved in the
898 observation medium and added to the cells in the observation medium at a selected final
899 peptide concentration at 37°C. Since their target sites are located on the cell surface, the
900 complex procedures employed for incorporating the FAM-Xpep-TATs inside the cells, as
901 described in the companion paper, were unnecessary.

902

903 **Ca^{2+} mobilization assay**

904 The Ca^{2+} mobilization assay was performed in basically the same way as described in the
905 companion paper. However, when we observed Ca^{2+} responses using the cells expressing
906 SNAPf-MOR, we employed the CHO-K1 cells stably expressing both Gqi5 and SNAPf-MOR (at
907 number densities of 0.75 ± 0.25 spots/μm^2 when labeled with SNAP-Surface549). To observe
908 the effect of DOR-Halo and KOR-Halo co-expression, the cells stably expressing Gqi5 and
909 SNAPf-MOR were transiently transfected with the cDNAs encoding these proteins. The cells
910 exhibiting spot densities of DOR-Halo or KOR-Halo at 0.75 ± 0.25 spots/μm^2 (after labeling
911 with Halo-SaraFluor650T) were selected for observations. Therefore, the Ca^{2+} mobilization
912 assay was performed at about the same low expression levels of ORs as those employed for
913 single fluorescent-molecule imaging experiments.

914

915 **Quantifying the internalization of SNAPf-ORs**

916 See the companion paper under the same title.[1]

917

918 **Systemic morphine administration to mice and examination of its antinociceptive**
919 **effect**
920 Morphine hydrochloride (Takeda Pharmaceutical) was dissolved in saline and subcutaneously
921 administered to mice once each day (10 mg/kg) for 11 days. Antinociception was measured
922 by the tail-flick test on days 1, 5, 8, and 11 from 0 to 120 min after morphine administration
923 (details will be described later). Body weight was measured before each morphine injection.
924 The control group received saline without morphine. All animal experiments were randomized
925 and performed by a blinded researcher, who was then unblinded before statistical analysis.
926
927 **Intracerebroventricular administration of the Dpep(20-42)DM peptide in mice**
928 The Dpep(20-42)DM peptide was dissolved in freshly prepared aCSF (127 mM NaCl, 1.5 mM
929 KCl, 1.24 mM KH_2PO4, 1.4 mM $MgSO_4$, 26 mM $NaHCO_3$, 2.4 mM $CaCl_2$, 10 mM D-glucose).
930 For continuous intracerebroventricular administration, an osmotic minipump (Alzet model
931 2002) filled with the peptide solution was implanted according to the manufacturer's protocol
932 and as described previously.[80] In order to stabilize the pump flow rate, the pumps were
933 primed by placing them in sterile saline at room temperature overnight. The osmotic
934 minipumps were filled with 200 μL of aCSF with or without the peptide solution (0.83 mg/mL
935 in aCSF). The minipump was connected to a 2.5-mm-long cannula (Alzet Brain Infusion Kit 3)
936 via a 1.5-cm-long polyvinylchloride tube. Before surgery, the mice were anesthetized with a
937 combination anesthetic (0.75 mg/kg of medetomidine, 4.0 mg/kg of midazolam, and 5.0
938 mg/kg of butorphanol). The scalp was shaved, Povidone-Iodine (Isodine, Mundipharma K.K.)
939 was applied, and an incision was made along the midline of the scalp; hemostats were then
940 used to make a pocket under the skin between the shoulder blades. The skull was scraped
941 clean of periosteum so that the cannula can properly adhere to the skull. A microdrill
942 (Tamiya, Inc.) was used to create a hole approximately 1.1 mm lateral and 0.5 mm caudal to
943 the bregma. The minipump was placed in the pocket under the skin between the shoulder
944 blades, the cannula was inserted through the drilled hole into the lateral ventricle, and the

945 cannula pedestal was affixed to the skull with cyanoacrylate glue and resin cement. The
946 incision was closed with soft silk sutures and antibacterial ointment was applied to the
947 wound. The animals were allowed to rest on a disposable heating pad until they were
948 recovered by using 0.75 mg/kg of atipamezole and then returned to their home cages in the
949 animal facility for 1-2 days until the measurement. Cannula placement into the lateral
950 ventricle was verified with trypan blue (4%, 10 μl).
951

952 **Morphine-induced antinociception assay**

953 Morphine-induced antinociception was evaluated by using the tail-flick test.[22] Using a tail-flick
954 apparatus (IITC Life Science), the intensity of the heat source was set at 10, which resulted
955 in a basal tail-flick latency of 2-3 s for most of the animals. The tail-flick latency was recorded
956 before (0 min, baseline latency) and every 30 min after morphine injection (30, 60, 90, and
957 120 min). The results are presented as a percentage of the maximal possible effect, %MPE,
958 which was calculated for each mouse at each time point according to the following formula:
959 %MPE = [(latency after drug − baseline latency)/ (10 − baseline latency)] × 100. Cutoff
960 latency was selected at 10 s to minimize tissue damage. The area under the %MPE vs. time
961 curve (AUC) for each treatment condition was also used to evaluate antinociception (Fig. 8h).
962 Normal distribution of the data was verified before performing the parametric statistical
963 analysis. Wherever appropriate, data were analyzed using two-way ANOVA, followed by
964 Tukey's post hoc tests or a multiple unpaired t-test with significance set at $P < 0.05$. All
965 calculations were performed using the GraphPad Prism 9 software (GraphPad Software).
966

967 **Software and statistical analysis**

968 The same as described in the companion paper.[1]
969

970 **Data availability**

All data generated or analyzed for this study are available within the paper and its associated Supplementary Information. Any additional information required to reanalyze the data reported in this paper is available from the lead contact upon reasonable request. Superimpositions of image sequences obtained in two colors and tracking single-molecules for in-vitro observation data were performed using C + +-based computer programs, produced in-house and based on the well-established approaches.[81] Further information regarding the experimental design may be found in the Nature Research Reporting Summary.

Code availability

Source codes for this have been integrated into a large, complex software package. While the software package cannot be extracted in a useful way, the entire software is available from the lead contact upon reasonable request, who will provide guidance on how to use it, as its manual and comments are written in Japanese.

Acknowledgements

We thank Profs. H. Takeshima of Kyoto University, R. Schülz of the University of Münich, and R. Y. Tsien of the University of California San Diego, for their kind gifts of cDNAs encoding rat KOR and DOR, that encoding rat MOR, and that encoding mCherry, respectively. We also thank Ms. Irina Meshcheryakova for technical help in preparing the cDNAs. This work was supported in part by Japan Society for the Promotion of Science (JSPS) Grants-in-Aid for Scientific Research (Kiban A to A.K. [21H04772], Kiban S to A.K. [16H06386], Kiban B to T.K.F. [16H04775, 20H02585], Kiban C to R.S.K. [17K07333], Wakate B to R.S.K. [26870292], Wakate to T.A.T. [21K15058], and Challenging Exploratory Research to T.K.F. [18K19001] and A.K. [22K19334]), a Grant-in-Aid from the Ministry of Education, Culture, Sports,

Science and Technology of Japan (MEXT) for Transformative Research Areas (A) to T.K.F. (21H05252), and a JST grant ACT-X to T.A.T. (JPMJAX211B). WPI-iCeMS of Kyoto University is supported by the World Premiere Research Center Initiative (WPI) of MEXT.

Contributions

P.Z., R.S.K., and A.K. conceived and formulated the project. A.K., T.A.T., T.K.F., and P.Z. developed the simultaneous dual-color single-molecule tracking station. P.Z. and A.K. designed biological experiments, and P.Z., with help from T.A.T., performed virtually all of the microscopic experiments. T.K.F., T.A.T., and A.K. developed and improved the in-house image analysis software and instrument control software, and discussed single-molecule imaging data. S.P. developed the theory for evaluating the dimer lifetimes from the single-molecule experimental data and assisted with its application to experimental results. T.A.T. and P.Z. analyzed the PCCF histograms and obtained dimer dissociation constants. W.F., with help from H.U., performed mouse experiments. P.Z., A.K., and T.A.T. wrote the manuscript, and all authors discussed the results and participated in the manuscript revisions.

Competing interests

PZ and AK have a patent pending for DpepDMs, MpepMDs and peptides from EL3 domains of ORs. The remaining authors have no conflicts of interest to declare.

References

1. Zhou, P., *et al.* Single-molecule detection of transient dimerization of opioid receptors 1: homodimers' effect on signaling and internalization. *Companion paper* (2024).

2. Fujita, W., Gomes, I., Devi, L.A. Revolution in GPCR signalling: opioid receptor heteromers as novel therapeutic targets: IUPHAR review 10. *Br. J. Pharmacol.* **171**, 4155-4176 (2014).

3. He, S. Q., *et al.* Facilitation of μ-Opioid receptor activity by preventing δ-opioid receptor-mediated codegradation. *Neuron* **69**, 120-131 (2011).

4. Keresztes, A., *et al.* Antagonism of the mu-delta opioid receptor heterodimer enhances opioid antinociception by activating Src and calcium/calmodulin-dependent protein kinase II signaling. *Pain* **163**, (2022).

5. Möller, J., *et al.* Single-molecule analysis reveals agonist-specific dimer formation of μ-opioid receptors. *Nat. Chem. Biol.* **16**, 946-954 (2020).

6. Milan-Lobo, L., Whistler, J. Heteromerization of the mu and delta opioid receptor produces ligand-biased antagonism and alters mu receptor trafficking. *J. Pharmacol. Exp. Ther.* jpet.111.179093 (2011).

7. Szafran, K., *et al.* Potential role of G protein-coupled receptor (GPCR) heterodimerization in neuropsychiatric disorders: a focus on depression. *Pharmacol. Rep.* **65**, 1498-1505 (2013).

8. Fribourg, M., *et al.* Decoding the signaling of a GPCR heteromeric complex reveals a unifying mechanism of action of antipsychotic drugs. *Cell* **147**, 1011-1023 (2011).

9. Kabli, N., Nguyen, T., Balboni, G., O'Dowd, B.F., George, S.R. Antidepressant-like and anxiolytic-like effects following activation of the μ-δ opioid receptor heteromer in the nucleus accumbens. *Mol. Psychiatry* **19**, 986-994 (2014).

10. Valentino, R.J., Volkow, N.D. Untangling the complexity of opioid receptor function. *Neuropsychopharmacology* **43**, 2514-2520 (2018).

11. Levac, B.A.R., O'Dowd, B.F., George, S.R. Oligomerization of opioid receptors: generation of novel signaling units. *Curr. Opin. Pharmacol.* **2**, 76-81 (2002).

12. Schmid, C.L., *et al.* Bias factor and therapeutic window correlate to predict safer opioid analgesics. *Cell* **171**, 1165-1175.e1113 (2017).

13. Darcq, E., Kieffer, B.L. Opioid receptors: drivers to addiction? *Nat. Rev. Neurosci.* **19**, 499-514 (2018).

14. Chan, H.C.S, McCarthy, D., Li, J., Palczewski, K., Yuan, S. Designing safer analgesics via μ-opioid receptor pathways. *Trends Pharmacol. Sci.* **38**, 1016-1037 (2017).

15. Cong, X., *et al.* Molecular insights into the biased signaling mechanism of the μ-opioid receptor. *Mol. Cell* **81**, 4165-4175.e4166 (2021).

16. Ferré, S., *et al.* G protein–coupled receptor oligomerization revisited: functional and pharmacological perspectives. *Pharmacol. Rev.* **66**, 413 (2014).

17. Pan, Z.Z. μ-Opposing actions of the κ-opioid receptor. *Trends Pharmacol. Sci.* **19**, 94-98 (1998).

18. Gomes, I., Gupta, A., Filipovska, J., Szeto, H.H., Pintar, J.E., Devi, L.A. A role for heterodimerization of μ and δ opiate receptors in enhancing morphine analgesia. *Proc. Natl. Acad. Sci. U.S.A.* **101**, 5135 (2004).

19. Gupta, A., *et al.* Increased abundance of opioid receptor heteromers after chronic morphine administration. *Sci. Signal* **3**, ra54-ra54 (2010).

20. Olson, K.M., Keresztes, A., Tashiro, J.K., Daconta, L.V., Hruby, V.J., Streicher, J.M. Synthesis and evaluation of a novel bivalent selective antagonist for the mu-delta opioid receptor heterodimer that reduces morphine withdrawal in mice. *J. Med. Chem.* **61**, 6075-6086 (2018).

21. Chefer, V.I., Shippenberg, T.S. Augmentation of morphine-induced sensitization but reduction in morphine tolerance and reward in delta-opioid receptor knockout mice. *Neuropsychopharmacology* **34**, 887-898 (2009).

22. Gomes, I., *et al.* Identification of a μ-δ opioid receptor heteromer-biased agonist with antinociceptive activity. *Proc. Natl. Acad. Sci. U.S.A.* **110**, 12072 (2013).

23. Wang, D., *et al.* Functional divergence of delta and mu opioid receptor organization in CNS pain circuits. *Neuron* **98**, 90-108.e105 (2018).

24. Zhu, Y., *et al.* Retention of supraspinal delta-like analgesia and loss of morphine tolerance in delta opioid receptor knockout mice. *Neuron* **24**, 243-252 (1999).

25. Egan, T.M., North, R.A. Both mu and delta opiate receptors exist on the same neuron. *Science* **214**, 923-924 (1981).

26. Wang, H. B., *et al.* Coexpression of δ- and μ-opioid receptors in nociceptive sensory neurons. *Proc. Natl. Acad. Sci. U.S.A.* **107**, 13117-13122 (2010).

27. Chakrabarti, S., Liu, N. J., Gintzler, A.R. Formation of μ-/κ-opioid receptor heterodimer is sex-dependent and mediates female-specific opioid analgesia. *Proc. Natl. Acad. Sci. U.S.A.* **107**, 20115-20119 (2010).

28. Jordan, B.A., Devi, LA. G-protein-coupled receptor heterodimerization modulates receptor function. *Nature* **399**, 697-700 (1999).

29. Berg, K.A., *et al.* Allosteric Interactions between δ and κ opioid receptors in peripheral sensory neurons. *Mol. Pharmacol.* **81**, 264 (2012).

30. Jacobs, B.A., *et al.* Signaling characteristics and functional regulation of delta opioid-kappa opioid receptor (DOP-KOP) heteromers in peripheral sensory neurons. *Neuropharmacology* **151**, 208-218 (2019).

31. Jacobs, B.A., Pando, M.M., Jennings, E., Chavera, T.A., Clarke, W.P., Berg, K.A. Allosterism within δ opioid-κ opioid receptor heteromers in peripheral sensory neurons: regulation of κ opioid agonist efficacy. *Mol. Pharmacol.* **93**, 376-386 (2018).

32. Waldhoer, M., *et al.* A heterodimer-selective agonist shows in vivo relevance of G protein-coupled receptor dimers. *Proc. Natl. Acad. Sci. U.S.A.* **102**, 9050 (2005).

33. Gomes, I., Ayoub, M.A., Fujita, W., Jaeger, W.C., Pfleger, K.D.G., Devi, L.A. G protein–coupled receptor heteromers. *Annu. Rev. Pharmacol. Toxicol.* **56**, 403-425 (2016).

34. Gurevich, V.V., Gurevich, E.V. GPCRs and signal transducers: interaction stoichiometry. *Trends Pharmacol. Sci.* **39**, 672-684 (2018).

35. Bellot, M., *et al.* Dual agonist occupancy of AT1-R-α2C-AR heterodimers results in atypical Gs-PKA signaling. *Nat. Chem. Biol.* **11**, 271-279 (2015).

36. Ferré, S., Ciruela, F., Woods, A.S., Lluis, C., Franco, R. Functional relevance of neurotransmitter receptor heteromers in the central nervous system. *Trends Neurosci.* **30**, 440-446 (2007).

37. Ngamlertwong, N., Tsuchiya, H., Mochimaru, Y., Azuma, M., Kuchimaru, T., Koshimizu, T.-a. Agonist dependency of the second phase access of β-arrestin 2 to the heteromeric μ-V1b receptor. *Sci. Rep.* **11**, 15813 (2021).

38. Jorand, R., *et al.* Molecular signatures of mu opioid receptor and somatostatin receptor 2 in pancreatic cancer. *Mol. Biol. Cell* **27**, 3659-3672 (2016).

39. Hübner, H., *et al.* Structure-guided development of heterodimer-selective GPCR ligands. *Nat. Commun.* **7**, 12298 (2016).

40. Callén, L., *et al.* Cannabinoid receptors CB1 and CB2 form functional heteromers in brain. *J. Biol. Chem.* **287**, 20851-20865 (2012).

41. Verma, V., Hasbi, A., O'Dowd, B.F., George, S.R. Dopamine D1-D2 receptor Heteromer-mediated calcium release is desensitized by D1 receptor occupancy with or without signal activation: dual functional regulation by G protein-coupled receptor kinase 2. *J. Biol. Chem.* **285**, 35092-35103 (2010).

42. Filizola, M., Devi, L.A. Structural biology: how opioid drugs bind to receptors. *Nature* **485**, 314-317 (2012).

43. Filizola, M., Olmea, O., Weinstein, H. Prediction of heterodimerization interfaces of G-protein coupled receptors with a new subtractive correlated mutation method. *Protein Eng. Des. Sel.* **15**, 881-885 (2002).

44. Dijkman, P.M., *et al.* Dynamic tuneable G protein-coupled receptor monomer-dimer populations. *Nat. Commun.* **9**, 1710 (2018).

45. Pan, Y. X. Expression of opioid receptors in mammalian cell Lines. In: *Opioid Research: Methods and Protocols* (ed Pan ZZ). Humana Press (2003).

46. Liu, X., Kai, M., Jin, L., Wang, R. Computational study of the heterodimerization between μ and δ receptors. *J. Comput. Aided Mol. Des.* **23**, 321-332 (2009).

47. Marino, K.A., Prada-Gracia, D., Provasi, D., Filizola, M. Impact of lipid composition and receptor conformation on the spatio-temporal organization of μ-opioid receptors in a multi-component plasma membrane model. *PLOS Comput. Biol.* **12**, e1005240 (2016).

48. Meral, D., *et al.* Molecular details of dimerization kinetics reveal negligible populations of transient μ-opioid receptor homodimers at physiological concentrations. *Sci. Rep.* **8**, 7705 (2018).

49. Grasberger, B., Minton, A.P., DeLisi, C., Metzger, H. Interaction between proteins localized in membranes. *Proc. Natl. Acad. Sci. U.S.A.* **83**, 6258-6262 (1986).

50. Yekkirala, A.S., Kalyuzhny, A.E., Portoghese, P.S. Standard opioid agonists activate heteromeric opioid receptors: evidence for morphine and [d-Ala(2)-MePhe(4)-Glyol(5)]enkephalin as selective μ-δ agonists. *ACS. Chem. Neurosci.* **1**, 146-154 (2010).

51. Fagan, R.R., Lee, D.F., Geron, M., Scherrer, G., von Zastrow, M., Ehrlich, A.T. Selective targeting of mu opioid receptors to primary cilia. *Cell Rep.* **43**, (2024).

52. Décaillot, F.M., Rozenfeld, R., Gupta, A., Devi, L.A. Cell surface targeting of mu-delta opioid receptor heterodimers by RTP4. *Proc. Natl. Acad. Sci. U.S.A.* **105**, 16045-16050 (2008).

53. Bao, F., Li, C.L., Chen, X.Q., Lu, Y.J., Bao, L., Zhang, X. Clinical opioids differentially induce co-internalization of μ- and δ-opioid receptors. *Mol. Pain* **14**, 1744806918769492 (2018).

54. Rozenfeld, R., Devi, L.A. Receptor heterodimerization leads to a switch in signaling: β-arrestin2-mediated ERK activation by μ-δ opioid receptor heterodimers. *FASEB J.* **21**, 2455-2465 (2007).

55. Grimes, J., *et al.* Plasma membrane preassociation drives β-arrestin coupling to receptors and activation. *Cell* **186**, 2238-2255.e2220 (2023).

56. Suzuki, K.G.N., Fujiwara, T.K., Edidin, M., Kusumi, A. Dynamic recruitment of phospholipase Cγ at transiently immobilized GPI-anchored receptor clusters induces IP3–Ca2+ signaling: single-molecule tracking study 2. *J. Cell. Biol.* **177**, 731-742 (2007).

57. Suzuki, K.G.N, Fujiwara, T.K., Sanematsu, F., Iino, R., Edidin, M., Kusumi, A. GPI-anchored receptor clusters transiently recruit Lyn and Gα for temporary cluster immobilization and Lyn activation: single-molecule tracking study 1. *J. Cell. Biol.* **177**, 717-730 (2007).

58. Kusumi, A., Tsunoyama, T.A., Suzuki, K.G.N., Fujiwara, T.K., Aladag, A. Transient, nano-scale, liquid-like molecular assemblies coming of age. *Curr. Opin. Cell Biol.* **89**, 102394 (2024).

59. Metcalf, M.D., *et al.* The δ opioid receptor agonist SNC80 selectively activates heteromeric μ-δ opioid receptors. *ACS. Chem. Neurosci.* **3**, 505-509 (2012).

60. Asher, W.B., *et al.* Single-molecule FRET imaging of GPCR dimers in living cells. *Nat. Methods* **18**, 397-405 (2021).

61. Cechova, K., Lan, C., Macik, M., Barthes, N.P.F., Jung, M., Ulbrich, M.H. Kappa but not delta or mu opioid receptors form homodimers at low membrane densities. *Cell. Mol. Life Sci.* **78**, 7557-7568 (2021).

1227 62. Drakopoulos, A., *et al.* Investigation of inactive-state κ opioid receptor
1228 homodimerization via single-molecule microscopy using new antagonistic fluorescent
1229 probes. *J. Med. Chem.* **63**, 3596-3609 (2020).
1230
1231 63. Baiula, M. Monitoring opioid receptor interaction in living cells by bioluminescence
1232 resonance energy transfer (BRET). *Methods Mol. Biol.* **2201**, 35-43 (2021).
1233
1234 64. Cvejic, S., Devi, L.A. Dimerization of the delta opioid receptor: implication for a role in
1235 receptor internalization. *J. Biol. Chem.* **272**, 26959-26964 (1997).
1236
1237 65. Gomes, I., Filipovska, J., Jordan, B.A., Devi, L.A. Oligomerization of opioid receptors.
1238 *Methods* **27**, 358-365 (2002).
1239
1240 66. He, L., Fong, J., von Zastrow, M, Whistler, J.L. Regulation of opioid receptor trafficking
1241 and morphine tolerance by receptor oligomerization. *Cell* **108**, 271-282 (2002).
1242
1243 67. Johnston, J.M., *et al.* Making structural sense of dimerization interfaces of delta opioid
1244 receptor homodimers. *Biochemistry* **50**, 1682-1690 (2011).
1245
1246 68. Manglik A*, et al.* Crystal structure of the μ-opioid receptor bound to a morphinan
1247 antagonist. *Nature* **485**, 321-326 (2012).
1248
1249 69. Kaneko, S., *et al.* Structural and dynamic insights into the activation of the μ-opioid
1250 receptor by an allosteric modulator. *Nat. Commun.* **15**, 3544 (2024).
1251
1252 70. Mahoney, J.P., Sunahara, R.K. Mechanistic insights into GPCR–G protein interactions.
1253 *Curr. Opin. Struct. Biol.* **41**, 247-254 (2016).
1254
1255 71. Whorton, M.R., *et al.* A monomeric G protein-coupled receptor isolated in a high-
1256 density lipoprotein particle efficiently activates its G protein. *Proc. Natl. Acad. Sci.*
1257 *U.S.A.* **104**, 7682-7687 (2007).
1258
1259 72. Nitsche, J.F, Schuller, A.G., King, M.A., Zengh, M., Pasternak, G.W., Pintar, J.E.
1260 Genetic dissociation of opiate tolerance and physical dependence in delta-opioid
1261 receptor-1 and preproenkephalin knock-out mice. *J. Neurosci.* **22**, 10906-10913
1262 (2002).
1263
1264 73. Xie, W. Y., *et al.* Disruption of Cdk5-associated phosphorylation of residue threonine-
1265 161 of the δ-opioid receptor: impaired receptor function and attenuated morphine
1266 antinociceptive tolerance. *J. Neurosci.* **29**, 3551 (2009).
1267
1268 74. Gaborit, M., Massotte, D. Therapeutic potential of opioid receptor heteromers in
1269 chronic pain and associated comorbidities. *Br. J. Pharmacol.* **180**, 994-1013 (2023).
1270
1271 75. Kasai, R.S., *et al.* Full characterization of GPCR monomer-dimer dynamic equilibrium by
1272 single molecule imaging. *J. Cell. Biol.* **192**, 463-480 (2011).
1273
1274 76. Tsunoyama, T.A., *et al.* Super-long single-molecule tracking reveals dynamic-
1275 anchorage-induced integrin function. *Nat. Chem. Biol.* **14**, 497-506 (2018).
1276
1277 77. Koyama-Honda, I., *et al.* Fluorescence imaging for monitoring the colocalization of two
1278 single molecules in living cells. *Biophys. J.* **88**, 2126-2136 (2005).
1279
1280 78. Murakoshi, H., *et al.* Single-molecule imaging analysis of Ras activation in living cells.
1281 *Proc. Natl. Acad. Sci. U.S.A.* **101**, 7317 (2004).

1282
1283 79. Fujiwara, T.K., *et al.* Confined diffusion of transmembrane proteins and lipids induced
1284 by the same actin meshwork lining the plasma membrane. *Mol. Biol. Cell.* **27**, 1101-
1285 1119 (2016).
1286
1287 80. Hagg. T. Intracerebral infusion of neurotrophic factors. In: *Neuroprotection Methods*
1288 *and Protocols* (ed Borsello T). Humana Press (2007).
1289
1290 81. Fujiwara, T.K., *et al.* Development of ultrafast camera-based single fluorescent-
1291 molecule imaging for cell biology. *J. Cell Biol.* **222**, (2023).